Scaling behaviours of karst networks around Tulum (Mexico): characterization, model and application.

A thesis presented

for the degree of

Doctor of sciences

by

Martin Hendrick

Faculty of Sciences

Center for Hydrogeology and Geothermics

(CHYN)

University of Neuchâtel, Switzerland

accepted on the recommendation of

Prof. Philippe Renard

Dr. Julien Straubhaar

Dr. Laurent Talon

Prof. Matt Covington

Defended on September 12^{th}, 2016

UNIVERSITÉ DE NEUCHÂTEL

Faculté des sciences
Secrétariat-décanat de Faculté
Rue Emile-Argand 11
2000 Neuchâtel - Suisse
Tél: + 41 (0)32 718 2100
E-mail: secretariat.sciences@unine.ch

IMPRIMATUR POUR THESE DE DOCTORAT

La Faculté des sciences de l'Université de Neuchâtel autorise l'impression de la présente thèse soutenue par

Monsieur Martin Hendrick

Titre:

“Scaling behaviours of karst networks around Tulum (Mexico): characterization, model and application”

sur le rapport des membres du jury composé comme suit:

- Prof. ass. Philippe Renard, directeur de thèse, Université de Neuchâtel, Suisse
- Dr Julien Straubhaar, Université de Neuchâtel, Suisse
- Prof. ass. Matthew D. Covington, University of Arkansas, USA
- Dr Laurent Talon, Laboratoire FAST, CNRS, Orsay, France

Neuchâtel, le 20 octobre 2016 Le Doyen, Prof. R. Bshary

Abstract

An unsolved problem in the field of karst networks is to understand and describe their large scale behaviours. The characterization of the structure of karst systems is crucial for many practical purposes, as for example, ground surface stability assessment and water resource management. However, there is no general framework that allows to fully characterize and model a network.

Natural systems often present scale invariant features. The objective of this thesis is then to initiate the characterization and the modelling of karstic structures based on scale invariances. We study, at different length scale, the properties of the mapped karst networks in the region of Tulum, Mexico. We find that these networks are well defined fractal structures. Based on this characterization, we build a model that is able to generate networks exhibiting similar scale invariances than those observed. We make the assumption that Tulum's karstic networks are structures that dissipate a minimal amount of energy due to friction forces for a minimal number of conduits. In the examined region around Tulum, there are still several unexplored areas where we expect to find similar karstic networks. Therefore, in a second step, our model is used to generate realistic networks that could be located in these zones. The aim of this last part is to simulate the networks in a region where they are unknown as a prerequisite to assess the aquifer's vulnerability which suffers from the development of tourism.

Keywords: karst network, fractal geometry, critical phenomena

Résumé

La compréhension de la structure et du comportement à grandes échelles des réseaux karstiques reste une question en suspens, bien que, la caractérisation de ces systèmes soit de première importance pour de nombreuses raisons pratiques liées à l'exploitation et à la préservation de la qualité de l'eau.

L'objectif de cette thèse est d'étudier les propriétés invariantes d'échelles des réseaux de karsts localisés dans la région de Tulum (Mexique). Nous avons mis en évidence la structure fractale de ces systèmes. Cette caractérisation nous a permis de construire un modèle réaliste de réseaux karstiques. Ce modéle nous apprend que la structure des réseaux de Tulum est telle qu'elle tend à minimiser l'énergie dissipée par friction dû à l'écoulement de l'eau tout en gardant une taille totale restreinte. Le modèle développé est ensuite utilisé pour étudier le transport de polluant et la vulnérabilité de la région de Tulum.

Mots-clefs: réseau karstique, géometrie fractale, phénomène critique

Acknowledgements

This work was funded by the Swiss National Science Foundation (project number 141298). The research carried out during this thesis would not have been possible without the courtesy of the Quintana Roo Speleological Survey who provides us a great and essential data set of high quality: the maps of the explored networks around the town of Tulum.

I would like to thank my PhD director, Philippe Renard, who gave me a considerable freedom and trust into my work all along my thesis. Thank you Philippe for your kindness during all these years!

For all those hours, sometimes exhausting but always great, spent on the field in Yucatan I would like to thank Axayacatl Maqueda (and also for all these Orval and discussions)!

My life in Switzerland would not have been the same without all my friends with who we spent a lot of times in mountains. Especially, I would like to thank Seb Gerber (thank you for all the hours of ski, climb and mountaineering all around the Alps) you taught me a lot! Tommy and Jeremy with who we did a great ski trip toward the Lygen Alps 3 month before sending the final manuscript of my thesis. It gave me a great amount of fresh air and energy for the last straight line of the redaction. Dylan, with who, one day, we decided to try dry tooling. We practised it with enthusiasms (during nights, under thunder), I'll never forget all these special moments. Thank you Chris for all those hours of bouldering and climbing always (or almost...) training hard. You are a great partner! I did my first steps on the crests of the Alps with Christian, thank you for all these nice climbs and the trust you have placed in me! Thank you Gregory Deman to teach me the basics of ski at the Bugnenets, it led me to ski up the Grand Combin, I will never forget it! I also would like to thank Eric for all the nice, after office day, ski adventures at the Chasseral, especially the wild one on the crest toward Le Rumont.

Dylan (one more time) and Luna: you were super nice room

(home)-mates, Le Pâquier miss me a lot, It was great to live there and to do music with you! I hope, one day, to live in a such nice place!

Olivier Stassart, who, one day, when I was revising my exam of supersymmetry, forwarded me the call for application for this thesis by email. Thank you for your thoughtfulness!

Thank you to, among others, Yes, Plaid, Popol Vuh, Gerard Grisey, Pink Floyd, Dr. Octagon, Marin Marais, Jethro Tull, Bach, Autechre, Couperin, Arnalds, Kapsberger, Deltron 3000, Pascal Dusapin, Stephen Steinbrink, Arvo Part, A Tribe Called Quest for your company all along my research work! Romain: thank you to share with me your passion for music and for all the great moments we spent together!

Thank you to Dan, Chris, Axa and James for your help to improve my manuscript! Gregory Kaeser you did a great work during your MSc, I hope it would prevent a bit the ecological disaster that is in the process around Tulum...

I would like to thank Professor Yves de Rop, your deep understanding and enthusiasm for physics is a continuous and considerable inspiration for me.

Thank you the family! Fred, Elo, Jona you were always present for me, thank you for your visits, your encouragements and all your attentions. Thank you J-C to give me interest and enthusiasm in sciences and research since my childhood.

Anna: thank you for all these great times spent to run, climb, do mountaineering or even chilling out and thank you to support me during the final phase of my thesis, you are a great and beautiful person, without you the life in Neuchâtel would no have been so NICE!

Contents

Chapter 1

Introduction

It is ubiquitous that the growth of the human population causes pressures on the environment and on the living beings, including humans themselves. To try to limit as far as possible, the inevitable impacts of the human activity, a collective ecological conscience has been developed since years. Scientists, among others, are involved and work for the preservation of our habitat. A great amount of work has been done in this way in many scientific disciplines like oceanography, biology, climatology, ... Physics and mathematics play a key role in the understanding of nature and therefore are a common foundation at the heart of these works.

In this thesis, we are interested in hydrogeology which is directly concerned by the study of the vulnerability of the water resource. We focus on groundwater. An important part of fresh water on earth, *i.e.* non saline water, is contained in the underground. The structure of flow path has to be studied through measurements adapted to probe groundwater. Such measurements rely on electromagnetism, acoustic, gravimetry, among others. Sometimes it is possible to access by ourselves to the subsurface, for example through caves. Caves, or more generally karst features, are present in limestone rocks. Water is able to dissolve limestone and create complex structures organized in a network in which water flows. However, only a small por-

Figure 1.1: The arrow indicates the location of the town of Tulum. Image adapted from Google map.

tion of these structures are explorable by humans because cave networks are not always well connected to the topography with sufficiently large entrances and passages allowing explorations. The understanding of how dissolution leads to the formation of extended networks in which water flow is crucial. In such environments, a pollution coming from the surface, is quickly spread.

Some regions of the world, like the Yucatan peninsula (Figure 1.1), are sustained in fresh water only through groundwater since the absence of surface water [Bauer-Gottwein et al. [2011]]. The Yucatan peninsula is a large limestone platform highly karstified, therefore a great part of the water flows in karst networks. We are mainly interested in the area of Tulum (located on the east part of the peninsula) which hosts the two extended submersed karst networks in the world Ox Bel Ha and Sac Actun (each one comprising more than 200 km of conduits). The study of this kind of structures brings into play, on a small scale, a local phenomena which is the dissolution process, from

which it emerges, on a large scale, a network transporting water over kilometers. Dissolution rates and local properties of rocks depend on space and time. In physics, such kind of systems, composed of many interacting components, are called complex systems.

1.1 Statistical physics and scale invariance

In principle, by integrating the equations of motion of a mechanical system made of a large number of particles, it is possible to fully determine it. However, it requires to solve a huge amount of equations and to specify a great number of initial conditions. It could be achieved using a computer that uses sophisticated algorithms aiming to minimize the propagation of numerical errors. When we are interested in macroscopic properties, *i.e.* on a length scale larger than its components, another approach should be considered.

One can think that the complexity of the properties of a system grows with its number of components. However, due to the complicated entanglement of numerous particles, a statistical behaviour may emerge on a macroscopic scale. The system, then, can be described by statistical laws that can not be reduced to purely mechanical law. The study of the statistical behaviour of a system is named statistical physics [Landau and Lifshitz [2013]].

Statistical physicists work on an abstract space named the phase space Γ. The phase space is the space of all the possible states of a system. A mechanical system is fully characterized when the positions and the impulsions of each of its constituting particles is known at each time. A state of a mechanical system at time t is represented by a point of the phase space (a point represents a set of N positions and N impulsions, with N the number of particles). The point follows a trajectory in the phase space when the system varies in time. Let's consider a

small part, but still comprising a large number of particles, of an isolated system. The behaviour of the subsystem is entangled in a complex way with the whole system. Statistical physics relies on the ergodicity hypothesis: if we observe over a large enough period T, the subsystem will explore many times each of its possible states. Therefore, the time averaged value on the period T of a function f of particles positions $q = (q_1, \ldots, q_N)$ and impulsion $p = (p_1, \ldots, p_N)$ is given by

$$\langle f \rangle \equiv \lim_{T \to \infty} \frac{1}{T} \int_0^T f(t)dt = \int_\Gamma f(q,p)\rho\left(q,p\right) dpdq \tag{1.1}$$

with ρ the probability density to observe the system in an given state and $\int_\Gamma \rho\left(p,q\right) dpdq = 1$. Macroscopic systems that are characterized by properties f equal to their averaged value $\langle f \rangle$ are named equilibrium systems.

For example, using the statistical physics framework, it is simple to study ideal gas (*i.e.* a system made of a great number of weakly interacting particles). We learned that the system is well described by the famous equation $PV \propto T$, with P, V and T respectively the pressure, the volume and the temperature of the gas. This is a statistical law that cannot be reduced to a mechanical law.

Continuous phase transition and scale invariance

Statistical physics is not limited to the study of dynamical systems. Let's introduce the Ising model which is at the heart of the study of ferromagnetism. The model is the following. A grid is occupied by particles, named spins, existing in two states, up (+) and down (-). Particles can not move and are fixed on grid's vertices, only their states is allowed to change. The system is fully determined knowing the state of each particle over the grid, this knowledge is represented by a point in the phase space Γ. We consider interactions between first nearest neighbour sites.

The total energy of the system is given by

$$E = -J \sum_{\langle ij \rangle} \sigma_i \sigma_j \tag{1.2}$$

with $J > 0$ the interaction constant, the sum is over pairs of first nearest neighbours spins $\langle ij \rangle$, and $\sigma_i = \pm 1$ the state (up $+1$ or down -1) of the site i. Therefore by minimizing its energy the system tends to create clusters of up or down spins.

We put the system in a thermal bath of temperature T. If the temperature is high, spins are disordered, *i.e.* state of spins are not correlated over the grid. If the temperature is small, interaction between spin occurs and an order appears. The order or the disorder is computed considering the magnetisation of the system

$$\langle m \rangle = \langle \sum_i \sigma_i \rangle \tag{1.3}$$

which is non zero only when the system is ordered. The magnetisation is the **order parameter** of the system. There is a particular temperature, named the **critical temperature** T_c, at which spins are correlated on all length scale (if we consider an infinite grid). The transition between ordered phase and disordered phase occurs at T_c and this is an example of **continuous phase transition**. The behaviour of the order parameter close to and bellow T_c is given by a power law

$$\langle m \rangle \propto \left(1 - \frac{T}{T_c}\right)^{\beta} \tag{1.4}$$

with β a universal exponent *i.e.* it depends only on the dimension of the grid and not on the grid's geometry. The exponent is $\beta = 1/8$ for 2-dimensional grids.

It is remarkable that close to the critical point the order parameter does not depend on the microscopic details of the system. In fact, the divergence of the correlation length at T_c induces a macroscopic collective behaviour (the magnetisation of the system) regardless the microscopic details.

Behaviour of systems close to the critical point, are described via functions following power laws (not only the order parameter). If different systems are described with the same set of exponents (one exponent for each function considered) one can say that they belong to the same universality class. A trivial example is the following. The Ising model can be defined on different grids geometry (square, triangular, ...). The critical temperature T_c depends on the grid configuration. However, the exponent describing the order parameter (and the others exponents describing the system) close to criticality stay the same (as long as we consider a 2-dimensional system). Therefore, in a trivial manner, the Ising models defined on different grids belong to the same universality class.

In fact, it is experimentally observed that some real systems, even if their microscopic characteristics (for example, nature of atoms or molecules) differ, may be described near criticality by the same set of power laws. Such kind of systems are said to belong to the same universality class. Therefore, systems can be categorized in different universality classes.

Power laws are features of scale invariants systems. Let's illustrate it. We consider a function f depending on x and which follows a power law $f(x) = cx^{\kappa}$. If we rescale the argument x by a constant factor b, we obtain $f(bx) = c(bx)^{\kappa} \propto x^{\kappa} \propto f(x)$. Therefore, regardless of the rescaling, the function has the same behaviour, it is scale invariant. Hence, the Ising model at T_c exhibit scale invariant properties.

While self-similarity looks as rather particular, many systems in nature have this remarkable property. Among other, river basins [Rodríguez-Iturbe and Rinaldo [2001]], leaf vein networks [Kenkel and Walker [1996]], snowflakes [Vicsek [1992]], shape of thunder light are structures exhibiting self-similarity. Self-similar objects are named fractals objects. The father of fractal geometry is Benoit B. Mandelbrot, who was the first to recognize scale invariance as an important feature characterizing natural systems [Mandelbrot [1983]].

Generic scale invariance

We have learned that the study of continuous phase transition is a way to generate structure exhibiting self-similarity. It exists other models showing scale invariant properties in a generic manner.

One of the most famous concept in the study of scale invariance is the Self-Organized Criticality (SOC) [Bak et al. [1987]]. The archetype system exhibiting SOC is the sandpile model. Grains of sand are randomly added one by one over a surface and form a pile. If the difference in elevation between two adjacent sites of the surface is above a given threshold, it may triggers an avalanche. More precisely, the added grain (the one which causes a difference in elevation above the threshold) topples its neighbours which increases their elevation and may cause other avalanches. The interest of the model relies on the observation that the avalanche properties such as the duration, the number of toppling or its area, show scale invariant features.

This model is historically one of the first to generate, from simple local interactions, a complex system exhibiting scale invariances that emerge generically, *i.e.* without the need of the tuning of a parameter. SOC is a feature of slowly driven out of equilibrium system (in our example the addition of grain one by one slowly drive the pile out of equilibrium). Models based on SOC has been used to study numerous phenomena, among others, earthquakes (the Olami-Feder-Christensen model [Olami et al. [1992]]) or forest-fires [Bak et al. [1990]].

An other outstanding example is the Kardar-Parisi-Zang equation (KPZ) which is a non-linear stochastic partial differential equation [Kardar et al. [1986]] describing the behaviour of an elevation field. This equation is useful to describe a large number of non-equilibrium systems that exhibit generic scale invariances, for example, growing crystalline surfaces and directed path in random media [Kardar and Zhang [1987]].

These two models exhibit generic scale invariances, *i.e.* without tuning a parameter to a particular value. Therefore, such

model evolves to criticality in a robust way. It is expected that natural systems are not driven to the critical point like we tune the temperature of the Ising model to the critical points. Therefore, they are interesting to model natural phenomena (except phase transition phenomena itself).

1.2 Objectives of the thesis

Karst systems are natural extended networks, formed by rock dissolution, that transports water over large scales. Since many natural systems exhibit self-similarities, it seems natural to try to assess karst networks' properties over scales and relate observed structures with already known critical models.

Our works is motivated by considering these questions:

- Do karst networks exhibit scale invariant properties?
- If yes, are we able to build a model of karst networks reproducing observed scaling properties?
- Can we understand, based on the model, the overall structure of karst networks?

With this aim, we study karst networks located around Tulum (Mexico). This area hosts numerous remarkably extended karst networks that have been intensively explored and mapped by cave divers.

We are interested in characterizing and modelling karst networks as fractal systems. We focus on the study of the connectivity property of karst networks. More explicitly we consider a karst system as a connected network leading to the transport of water over the space. The most natural framework to consider connected clusters in heterogeneous environment is the percolation theory (introduced in Chapter 2). This model, as the Ising model, has a critical point where the system undergoes a phase transition. Therefore, we are interested in properties of

percolation clusters (more precisely subnetworks of percolation clusters) near the critical point. Thus our model does not rely on a generic scale invariant model, however we motivate the parameters tuning by a global minimization principle.

1.3 Current state of the research

Models exhibiting self-similar properties have been proposed to study a variety of natural systems. For example, in Rodríguez-Iturbe and Rinaldo [2001], the authors built a model of river networks inspired by Self-Organized criticality. River networks emerge from the erosion of the topography by water. The topography is simplified as an elevation field over a grid. First a network is generated from a given initial topography as the tree (a loopless connected graph) connecting first nearest neighbours whose links are the drainage directions. More precisely, two grid's sites are linked if the elevation gradient between them is the steepest one among the possible choice. Therefore, on such topography water flows along the tree. At each site a shear stress τ, defined to be proportional to the elevation gradient and the flow rate[1], is computed. If at the site j, the shear stress τ_j is above a fixed threshold value τ_c, the elevation of j is lowered such that $\tau_j = \tau_c$, it is the erosion. Based on this new elevation field the drainage tree is updated. The process (erosion) is repeated until the system presents no more sites above the threshold. Topological and geometrical properties of networks generated by this mechanism are similar to those of real river networks. Moreover, they show that the total energy expenditure E (which is $E \propto \sum_j A_j^{1/2}$, A_j is the drained area by the site j) of the system is lowered by the erosion process. Thus, this model based on simple local interactions helps to understand how emerges an organized large scale network that optimizes the transport of water in terms of dissipated energy.

[1]The flow rate of the site j is proportional the drained area by the site j.

There are in the literature many of models to investigate scale invariance appearing in natural phenomena. Landscape erosion has also been studied via a stochastic partial differential equation (close to the KPZ equation) that describes the height (altitude) of the landscape [Pastor-Satorras and Rothman [1998]]. In geophysics, behaviours of faults have been studied through stochastic mechanics based on threshold dynamics [Smalley et al. [1985]]. The Ising model and Self-Organized Criticality are employed to study the functioning of the brain [Fraiman et al. [2009], Chialvo [2004]]. Flow and transport phenomena through porous media also have also been considered in the framework of percolation theory [Sahimi [2011], Martys et al. [1991], Stanley and Coniglio [1984]].

However, there is a gap in the literature related to the karst science. Karst networks has been characterized as fractal structures [Laverty [1987], Kusumayudha et al. [2000], Jeannin et al. [2007], Pardo-Iguzquiza et al. [2011]]. Different kind of models (deterministics, stochastics or pseudo genetics) have been proposed to simulate the formation or geometry of karst networks structure [Groves and Howard [1994], Dreybrodt et al. [2002], Jaquet et al. [2004], Borghi et al. [2012], Collon-Drouaillet et al. [2012], Pardo-Iguzquiza et al. [2012]]. The percolation model was considered to study dissolution mechanism at the origin of karst networks but without paying attention to the overall network structure [Siemers and Dreybrodt [1998]]. In this thesis, our aim is to initiate the study and model of the structure of karst systems as self-similar systems directly inspired by critical phenomena.

1.4 Structure of the thesis

In Chapter 2, we introduce the Tulum's karst networks and their environments. Next, we define concepts related to the study of systems exhibiting scale invariances. We explicitly motivate and define our approach of karst networks. The Chapter 3,

based on Hendrick and Renard [2016], and Chapter 4 are focused on the characterization of structural scale invariant properties of Tulum's karst networks. In Chapter 5, we propose a new model that aims to reproduce the structure of karst networks. In Chapter 6, we present an application of the model to a real problem and finally, chapter 7 contains the discussions and the conclusions about this work.

Chapter 2

Karstic networks and scaling behaviours

2.1 Introduction

In this Chapter, we introduce the background material that is used in this thesis. We first present the karst networks of the area of Tulum, Mexico. Then, we provide a summary of the methods and tools that we will use for the study of scaling behaviours.

Note that it exists various ways to study the structure of karstic systems. One way is to integrate a full mathematical description of dissolution processes that leads to the formation of the network taking into account a realistic geological environment. Such approaches are computationally heavy and have to face with problems such as numerical errors, definitions of realistic initial and boundaries conditions. These issues blur the understanding of the overall behaviour and organization of karst networks. Moreover, a precise characterization of "what is the structure of a karst network" is still missing, thus it is hard to asses if generated networks are realistic or not.

Another way to learn about karstic network structures relies on detailed morphometrics measurements carried out on sites or directly computed on caver's map of the systems. Such informa-

tions help to get an idea of the complexity and the organization of systems from conduits scale to the complete network [see for example Pardo-Iguzquiza et al. [2011]]. However, generally, it is hard to relate observed morphometric values with the responsible physical processes.

In this work, we compute basic karst network characteristics such as its dimension, random walk and conductivity behaviours. More precisely we focus on their scaling behaviours and on the associated exponents which are the **fractal dimension**, the **walk exponent** and the **conductivity exponent**. Such properties can be related to well studied physical models and help us to built an informative model of karst network structures and developments.

We structured the Chapter in the following parts. In Section 2.2, we briefly describe karst systems of Tulum and their environments. In Section 2.3, we introduce the notion of fractal dimension, walk exponent, conductivity exponent and the Einstein relation. We also define the percolation model which is at the heart of Chapter 5. Section 2.4 contains a discussion putting karst networks in the light of scaling transforms.

2.2 Karst networks of the area of Tulum

2.2.1 Overview of the region

The town of Tulum is located in the Yucatan peninsula in the state of Quintana Roo, Mexico (Figure 1.1). The peninsula is surrounded by the Mexican gulf and the Caribbean sea. It is an extended flat limestone platform covering, approximatively, an area of $300 \times 200\ km^2$. Most of water flows occurs in the underground. The peninsula is covered by *cenotes* which are sinkholes resulting from the collapse of underground caves. A recent review of the hydrogeology of the Yucatan peninsula can be found in Bauer-Gottwein et al. [2011].

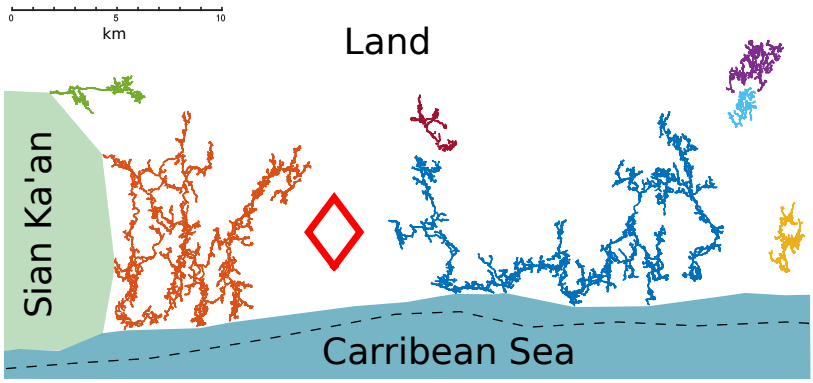

Figure 2.1: Sketch of the studied area. The red diamond symbolizes the location of the town of Tulum. The dotted line represents the coral reef. Spatial graphs are cave divers maps of karst networks.

The area of Tulum hosts numerous vulnerable ecological systems as wetlands, tropical forests as coral reefs. In the vicinity of Tulum is located the Sian Ka'an biosphere which is a natural reverse covering about 3200 km^2. The town is situated at approximatively 5 km from the sea shore which is home of the Mesoamerican barrier reef (Figure 2.1).

The economical development of the region relies on tourism which cause pressures on the environment [Juarez [2002]]. One of the major impacts is marked on the water quality. Only a small part of the wastewater is treated. Regardless of whether the wastewater has been treated or not, it is directly injected in the underground or in cenotes.

There is no established groundwater protection area. This is critical because drinking water comes from the underground. There is almost no soil on the surface of limestone rocks in this region, therefore groundwater is the main source of water for the natural habitats.

Figure 2.2 shows a striking example of the weakness of the groundwater management. One can see a new garbage discharge that as been built in 2015 which is directly situated upstream

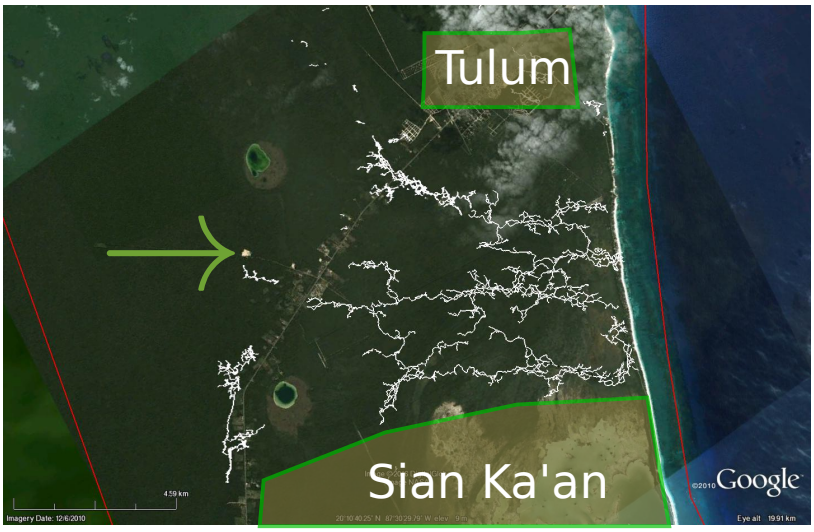

Figure 2.2: The arrow indictes the emplacement of the garbage discharge.

of the most extended flooded karst network in the world Ox Bel Ha. Any leak coming from the discharge will be spread by the karst network over kilometres toward the sea. Moreover, the discharge is situated at the border of the Sian Ka'an reserve.

The quality of the fresh water is also impacted by sea water intrusion which occurs over tens of kilometres from the sea shore. Fresh water, coming from precipitation, forms a lens over the intrusion saline water (due to density difference between the two bodies). The width of the lens vary from 1 m close to the sea to 100 m inland. In Tulum, the thickness of the lens is around 18 m which already deteriorates the quality of pumped water.

A NGO, Amigos de Sian Ka'an[1], works to the protection of the environment in this area. They sensitize people to the vulnerability of their environment and collaborate with scientists to better understand the interaction between the ecological systems covering this region.

[1]http://www.amigosdesiankaan.org/en/

2.2.2 The karst networks of the area

Karst features result from the dissolution of rocks by water. Dissolution process creates complex networks in which water flows. Numerous extended submersed networks have been mapped by cave divers around Tulum (Figure 2.1).

Karst networks in this area are shallow systems (mostly horizontally extended) connected to the sea. Sea level changes (over geological time) and sea tides impacts on the dissolution process. The mixing zone between fresh and salt water is one of the main dissolution source that creates caves and conduits [Kambesis and Coke IV [2013]].

The geology in which karst networks are embedded is rather simple [Smart et al. [2006]]. It is organized in horizontal layers (no folding due to tectonic movements) of immature limestone. Small scale fractures (meter scale) are observed. No large scale fracture or faults constrained the structure of the networks around Tulum. The only known major fracture zones is situated upstream of our study area. Therefore, on networks' scale, the geology is assumed to be homogeneous. The topography around Tulum is nearly flat and the regional hydraulic gradient is low ranging from 1 to 10 cm/km [Bauer-Gottwein et al. [2011]].

Conduits are wide, from 2 m to 30 m in diameters. They present speleothem features as stalagmites or stalactites. This is an indication that in their complex history, the karst networks, due to sea level changes (occurring due to glacial and interglacial period), were exposed to the air.

Breakdown piles of rock are commonly observed in conduits resulting from small local collapses. Large collapses form skinholes (cenotes) that open the network to the surface. There is a huge amount of cenotes in the Yucatan peninsula. For example, the Ox Bel Ha counts 141 of cenotes for a total networks length of 260 km. It represents one entrance every 1.9 km, which is a penetration length manageable for experienced cave divers. The presence of numerous cenotes explain why networks are well explored in this area.

2.2.3 Cave divers' maps

Basically, a karst network is mapped step by step. The first step (station) is one of the entrance of the system. This station is geolocalized using a GPS. From this point, the caver steps to the next station which has to be connected to the first station by a straight line clear from any obstacle. Thus, the azimuth from the first point to the second one can be measured using a compass. Moreover, the depth of the station is recorded. This process is repeated to map the explored part of a network.

Often the network has many entrances. Thus, the set of GPS coordinates of the entrances helps to asses the accuracy of the mapping. One can also check if loops travelled by divers are properly closed. When the mapping is done, data are reported on the land map (Figure 2.2). The so produced karst networks, thanks to the detailed work of cave divers, are very accurate. The Quintana Roo Speleological Survey[2] lists all maps generated by different teams exploring networks in this area.

These maps are among of the best data sources to study the spatial organization of extended networks, not only around Tulum, since cavers produce maps of karst networks (dry or submersed) all over the earth.

In this work, we focus on the maps of explored karst networks of the area of Tulum (Figure 2.1). A karst network map is a spatial graph (cf. Section 2.2.4). The embedding space is simple since the stratification of the area is flat and looks homogeneous at the scale of the size of the networks. Our study is limited to explored and explorable parts of karst networks, due to the finite size of cave divers and the necessity of an entrance to access them. We study these maps throught different length scales in order to gain information about the structures of networks.

[2]https://caves.org/project/qrss/qrss.htm

2.2.4 Cave divers' maps and graph theory

A **graph** is a set of N nodes and a set of l links. Links are defined as pairs of nodes (ordered or not). In this work, we consider graphs without ordered links and self-loops (a self-loop is a link connecting a node to itself without intermediate nodes). The **degree** of a node is the number of incident links to the node. The degree at node a is denoted by $k(a)$. A **path** between two nodes is a set of distinct links, that connects them. A graph is said **disconnected**, if at least, it exists a pair of nodes that are not connected by a path. And thus, a graph is **connected** if every nodes are reachable following paths. A **loop** (or more precisely a cycle) is a closed path. A closed path is a path starting and ending at the same nodes. Nodes can be located in space. The resulting structure is named a **spatial graph**. All these definitions are illustrated in Figure 2.3.

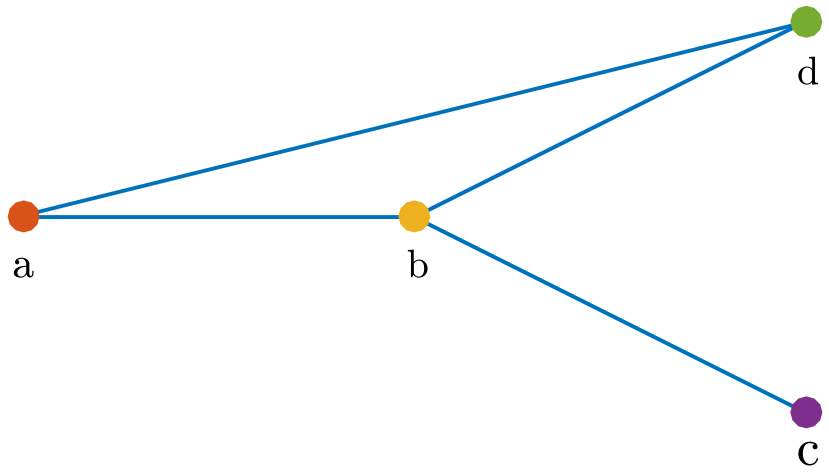

Figure 2.3: This connected graph is made of $N = 4$ nodes (labelled a, b, c and d), $l = 4$ links and one loop (the path $\{(a,b),(b,d),(d,a)\}$). Node's degree are $k(a) = 2$, $k(b) = 3$, $k(c) = 1$ and $k(d) = 2$.

This vocabulary helps to characterize maps of cave divers. Maps are connected spatial graphs. Since divers cartography

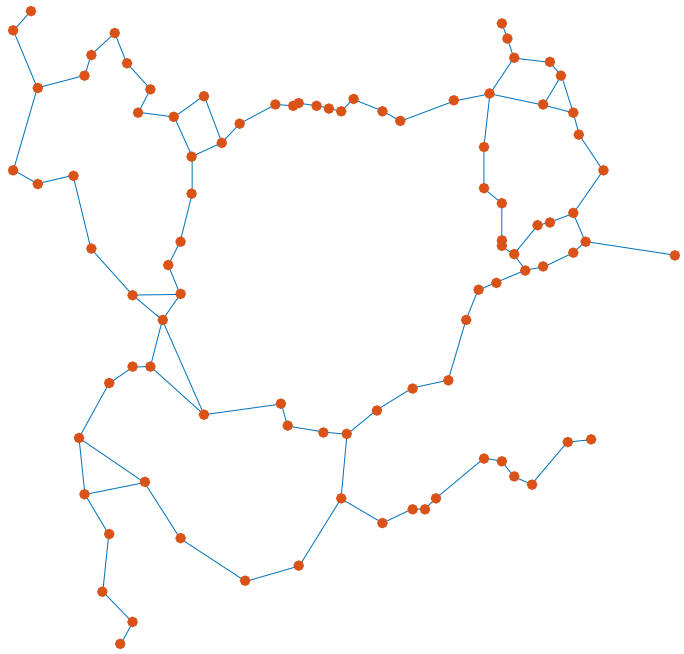

Figure 2.4: A small of a part typical cave diver map. Links length are around 4 meters. One can notice the presence of many loops of different sizes which underline the heterogeneity of flow path at local scale.

networks stepping from one station to another there is no self-loop. Figure 2.4 provides an example of a small part of an explored network. We can notice, that the distribution of node degree and link sizes (the Euclidean distance between to linked node) is narrow. This kind of networks is said to be homogeneous (in terms of topology and geometry) in contrast to, for example, the network of commercial flights between airports across the world. This network is characterized by an heterogeneous degree and link size distributions. Some nodes, named hubs (located at international airports), are characterized by a large degrees. Local airports present only few connections and thus are nodes of small degrees. Moreover, links length varies from local flights to long-haul flights.

A famous class of heterogeneous networks exhibits a power law degree distribution and is named scale-free networks [Barabási and Albert [1999]], the World Wide Web is an example.

There is a vast literature about networks and model of networks. An oustanding overview concerning spatial network models and characterizations is provided by Barthélemy [2011].

2.3 Scaling behaviours

2.3.1 Deterministic fractal

Symmetry is a key concept in physics. Systems are studied considering how their properties are modified by symmetry transformations. Let's illustrate the power of symmetry considerations on an example. A dynamical system is fully characterized by a functional named its action. By Noether's theorem the invariance of the action under a smooth (differentiable) symmetry transformation correspond to a conservation law. For example, the conservation of the energy of a system results in the invariance of its action under time translations.

In this work we are concerned by scale transforms and scale invariance of systems (without considering dynamical aspects). Therefore, we analyse and compare systems at different length scale.

A system is scale-invariant if its properties are unchanged under scale transformations. Thus, we are interested in self-similar structures. Self-similarity can be observed exactly (it is the case for deterministic fractal) or in a statistical sense (which is the case for random fractal). In the following, we define the tools that will be useful for the study of systems through scale. This Section is based and adapted from Ben-Avraham and Havlin [2000].

Fractal dimension

One of the most common characteristic of a system is its spatial dimension. Here, we introduce a convenient way to define and compute the dimension of an object trough the calculation of its box dimension. Let S be an object embedded in $\mathbb{R}^d$, the real space of dimension d. The box dimension d_f of S is defined as

$$d_f = \lim_{\epsilon \to 0} \frac{\log N(\epsilon)}{\log (1/\epsilon)} \tag{2.1}$$

with $N(\epsilon)$ being the minimal number of boxes of dimension d and size ϵ needed to cover S.

Let us illustrate this definition on a simple example. We consider a 2 dimensional square grid of total length λ. A box covering of the lattice is built iteratively (Figure 2.5). The grid at the first iteration appears as a unique square and can be covered by a unique square box. At the second iteration, the grid is made of 4 squares and hence is covered with 4 boxes of sizes $\epsilon = \lambda/2$. Thus, at iteration $k+1$, box size is $\epsilon = \lambda/2^k$ and the minimal number of boxes needed to cover the lattice is $N(\epsilon) = 4^k$. Supposing that the limit of the Equation (2.1) exists, we have

$$d_f = \lim_{k \to \infty} \frac{\log 4^k}{\log (2^k/\lambda)} = 2. \tag{2.2}$$

The covering at iteration k can be viewed as the coarse graining of the lattice at the iteration $k+1$. Therefore, each iteration is a representation of the lattice at different length scale and hence, is characterized by the same box dimension as the lattice. Thereby, we have $N(k+1) \propto \epsilon(k+1)^{-df}$ and $N(k) \propto \epsilon(k)^{-df}$, taking the ratio we obtain

$$\frac{\log \left(N\left(k+1\right)/N\left(k\right)\right)}{\log b} = 2 = d_f, \tag{2.3}$$

with the **renormalization parameter** $b = \epsilon(k)/\epsilon(k+1) = 2$. Compare an object through different length scale is an illustra-

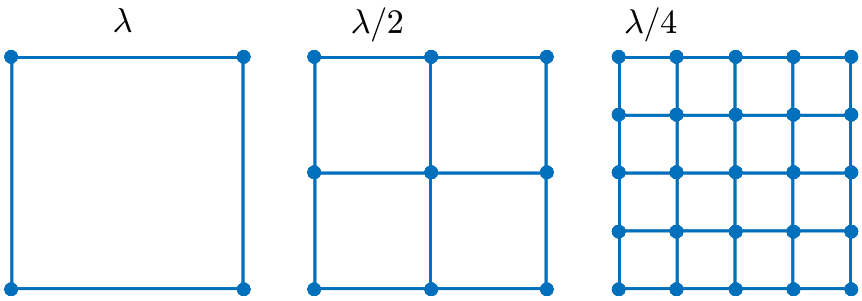

Figure 2.5: A covering of a square grid built iteratively.

tion of a procedure named real space renormalization. Renormalization was pioneered by Leo Kadanoff (see for example Kadanoff [2010] and formalize by Wilson [Wilson [1971]). It is easily understandable that renormalization is a powerful tool to asses self-similar systems. Renormalization is at the heart of nowadays physics like the study of critical phenomena [Täuber [2014]] and others field theories [Zinn-Justin [2007]].

Next, we compute the box dimension for a less trivial case. We consider the two dimensional Sierpinki gasket. It can be generated iteratively as follows (Figure 2.6). The initiator is an isometric triangle. From it, we remove an isometric triangle whose vertices (nodes) located at the middle of each edges (links) of the initiator. Each of the tree new triangles is considered as a new initiator and the process is repeated infinitely. The computation of the box dimension of the Sierpinski gasket

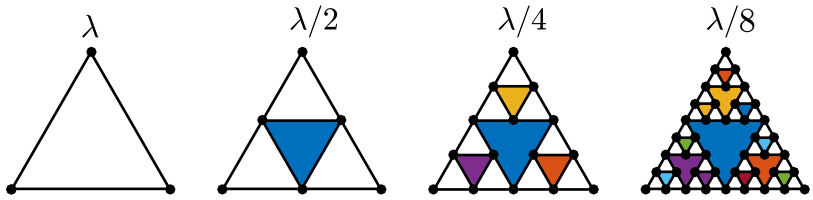

Figure 2.6: Construction of the 2 dimensional Sierpinski gasket.

is direct. Consider triangular boxes. The Sierpinski gasket at

iteration 1 is covered by a unique box of length λ. At literation 2, three boxes of size $\lambda/2$ are needed to tile it. Hence, supposing that the limit of Equation (2.1) exists, we have

$$\lim_{k\to\infty} \frac{\log 3^k}{\log\left(2^k/\lambda\right)} = \frac{\log 3}{\log 2} = d_f \tag{2.4}$$

Equivalently we can compute d_f assuming that the iteration k the coarse graining of the iteration $k+1$, this gives directly

$$d_f = \frac{\log 3}{\log 2} \approx 1.59. \tag{2.5}$$

By construction, the Sierpinski gasket is a self-similar deterministic structure (up to the upper cutoff length scale λ). Due to the presence of holes at all length scales it is a sparser object than a 2 dimensional structure. Meanwhile the length of the path linking two nodes is infinite thus it is a denser object than a 1 dimensional system. Thus, the dimension of the Sierpinski lower than 2 but larger than 1.

Walk exponent

Fractal objects can be further characterized by studying the behaviour of random walkers on those structures. We begin with the study of a random walk on an infinite 2-dimensional square lattice, of size λ (the distance between two nodes). The walk is initiated at a randomly selected node. The walker steps randomly on one of the four nearest-neighbours of the initial node. The process is repeated until the walker made t steps (the duration of the walk). The displacement of the walker after t steps is

$$\boldsymbol{r}(t) = \sum_{i=1}^{t} \boldsymbol{e}_i, \tag{2.6}$$

each $\boldsymbol{e}_i$ are vectors corresponding the displacement at the step i. At each step, it is equally likely to hop to one of next nearest

nodes, thus provided enough steps we have

$$\langle \boldsymbol{r}(t) \rangle = \sum_{i=1}^{t} \langle \boldsymbol{e}_i \rangle = \mathbf{0}, \tag{2.7}$$

with $\langle \cdot \rangle$ the average over many walks of duration t. It is interesting to study the mean square displacement (the variance of the walk)

$$\langle r^2(t) \rangle = \langle \left(\sum_{i=1}^{t} \boldsymbol{e}_i \right)^2 \rangle = \lambda^2 t + 2 \sum_{i>j}^{t} \langle (\boldsymbol{e}_i \cdot \boldsymbol{e}_j) \rangle = Dt \tag{2.8}$$

with $(\cdot)$ the Euclidean scalar product and $\langle (\boldsymbol{e}_i \cdot \boldsymbol{e}_j) \rangle = 0$ due to the independence of step i and j if $i \neq j$. The constant $D \equiv \lambda^2$ is called the diffusion coefficient. Therefore, the mean square displacement of the random walker scales proportionally with t

$$\langle r^2(t) \rangle \propto t \tag{2.9}$$

The continuous time and space limit of this process is named diffusion. It is worth to notice that Equation 2.9 holds for any regular (*i.e.* non fractal) lattice in any integer dimension.

Random walks on fractal objects behave differently. Let's illustrate this issue on the 2 dimensional Sierpinski gasket. The Siperpinki gasket can be viewed as embedded in a regular triangular lattice. All nodes of the lattice are equivalents. It is not the case for the Sierpinski gasket. Depending on which node we consider, two edges of the triangular lattice may be missing. The degree of a node depends on its location (Figure 2.6). It follows that two steps of the random walk are correlated, *i.e.* $\langle \boldsymbol{e}_i \cdot \boldsymbol{e}_j \rangle \neq 0$. The mean square displacement is not any more proportional to the displacement time, but is given by

$$\langle r^2(t) \rangle \propto t^{2/d_w} \tag{2.10}$$

with d_w being the walk exponent.

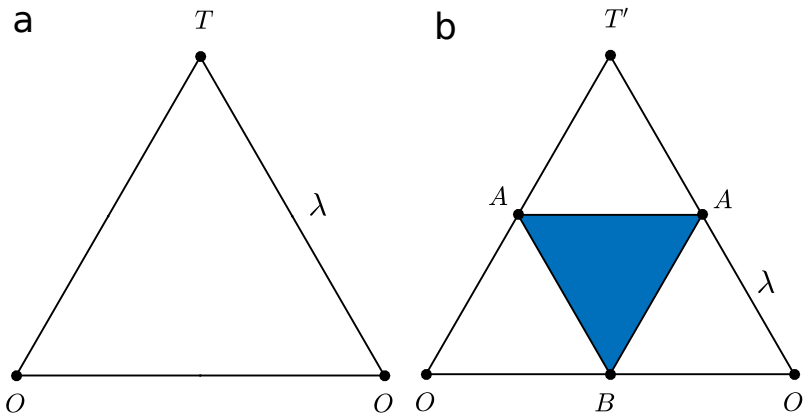

Figure 2.7: (a) and (b), respectively iteration 1 and 2 of the Sierpinki gasket. Notice that, space coordinates are rescaled in order to fix the link length to be λ.

The walk exponent of the Sierpinski gasket can be computed exactly. We study the mean first-passage time needed to walker to step from the top node to one of the bottom nodes. The first-time passage is the time needed to visit for the first time a given set of nodes. We compare walker's behaviour on the iteration 1 and 2 of the Sierpinski gasket (Figure 2.7). Notice that, here, space coordinates are rescaled since we want to study the random walk trough length scale (the distance between two nearest nodes is keep fixed at λ). On iteration 1 the mean first-passage time is T and it represents the time needed to perform one step. The intermediate mean first-passage times, on iteration 2, are denote A and B. We express T', A and B in function of T [3]. We have

$$\begin{aligned} T' &= T + A \\ A &= \frac{1}{4}(T + T') + \frac{1}{4}(T + A) + \frac{1}{4}(T + B) + \frac{1}{4}T \\ B &= \frac{1}{2}T + \frac{1}{4}(A + T) + \frac{1}{4}(A + T) \end{aligned}$$

[3]Notice that the nodes are labelled by the corresponding mean first-passage time

The walker steps randomly, thus, for example the probability to move to the next node being at A is $1/4$. For example, from A there is a probability $1/4$ to move up to T' and hence cumulate a first-passage time walk of $T + T'$, and so on. Solving the linear system gives $T' = 5T$, $A = 4T$ and $B = 3T$. Let L^2 be the mean square displacement of the walker on the Sierpinski gasket at iteration 1. Hence, given Equation (2.10)

$$L \propto T^{1/d_w} \tag{2.11}$$

The iteration 1 is the coarse graining of the iteration 2 of the Sierpinski gasket. They are the same object transformed by a real space renormalization procedure. Therefore, their properties are transformed in correspondence to the rescaling of the space coordinate by $b = 2$

$$L \quad \rightarrow \quad L' = bL = 2L$$

which correspond to a rescaling of time

$$T \quad \rightarrow \quad T' = 5T$$

We have $L' \propto T'^{1/d_w}$, since we consider the same object. Thus, the walk exponent can be computed

$$d_w = \frac{\log T'/T}{\log L'/L} = \frac{\log 5}{\log 2} \approx 2.32. \tag{2.12}$$

Conductivity exponent

Basic transport ability of a network can be studied by assigning a resistor to each link. It enables us to study interesting properties such total resistance or dissipated energy. In the following, we study transport property of the Sierpinski gasket. We assuming on each link a flow rate described by the Hagen-Poiseuille equation $\Delta P = -RQ$ with ΔP, R and Q being, respectively, the pressure drop, the resistance and flow rate.

Since fractal objects are self-similar structures it is expected that the resistance between two nodes separated by an Euclidean distance of L follows a power law, *i.e.*

$$R \propto L^{\tilde{\zeta}}. \tag{2.13}$$

We compute the total resistance by injecting a current I at the top node and measuring the outcome at one of the bottom nodes (Figure 2.8). Again, we compute it for iteration 1 and 2 of the Sierpinki gasket. In Figure 2.8B the total resistance R' given by

$$R' = R + \left(\frac{1}{R} + \frac{1}{2R}\right)^{-1} = \frac{5}{3}R \tag{2.14}$$

Considering the rescaling of the length scale by $b = 2$ we have

$$\begin{aligned} L &\rightarrow L' = 2L \\ R &\rightarrow R' = \frac{5}{3}R \end{aligned}$$

Therefore,

$$\tilde{\zeta} = \frac{\log 5/3}{\log 2} \approx 0.737 \tag{2.15}$$

It worth to notice that the three exponents, d_f, d_w and $\tilde{\zeta}$ are not independent. They are linked by the 2-dimensional Einstein relation, $\tilde{\zeta} = -d_f + d_w$ (cf. Section 2.3.1).

Einstein relation

Here we follow again Ben-Avraham and Havlin [2000] to derive the Einstein relation using the electronic-hydraulic analogy.

The Einstein relation links the conductivity σ to the diffusion constant D and the medium density n such that

$$\sigma \propto nD \tag{2.16}$$

Imagine we follow a representative elementary volume (REV) of water, or equivalently a passive tracer particle, in a pipe

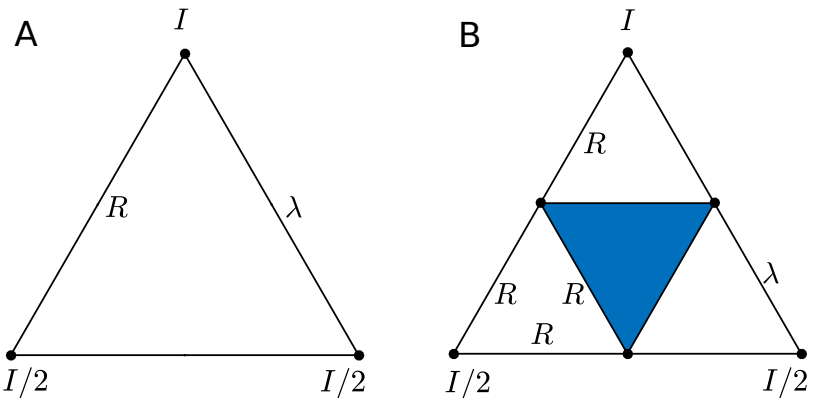

Figure 2.8: (A) and (B), respectively iteration 1 and 2 of the Sierpinki gasket. The resistance carried by a link is noted R. The total injected current is I, the measured current at the bottom nodes is $I/2$.

network. We impose a water height (pressure) difference to the 'borders' of the network (it is the global potential difference imposed on the system). For instance, the borders are edges of a busbar configuration (Figure 2.9). In each pipe, we assume, a linear flow given by the Hagen-Poiseuille equation $\Delta P/l = -Q/(\sigma_l a)$ with l, σ_l and a being the length, the conductivity and the cross section of the link, respectively. To assess the boundary conditions, we locate, the network on the positive plane $x > 0$ and assume a large linear size $L >> l$ of the network.

Let's take the continuum limit of this network, *i.e.* assume a large number of pipes in a limited domain (the busbar configuration). Hence, the path followed by the REV can be studied as a particle experiencing a biased diffusion. The bias is the drift experienced by the REV due to the global potential (water height difference) imposed on the network. The behaviour of the REV is described by the continuity equation

$$\frac{\partial p(x,t)}{\partial t} = -\frac{\partial}{\partial x} J(x,t) \tag{2.17}$$

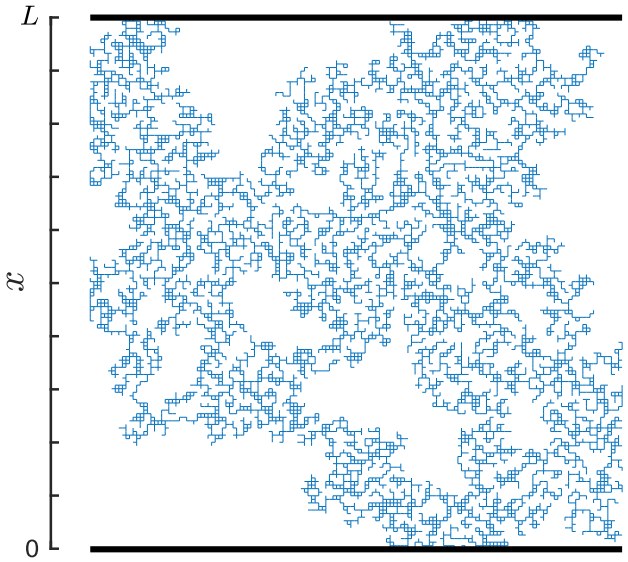

Figure 2.9: The busbar configaration. A fix pressure drop is applied between the upper and the bottom edges (tick lines).

with $J \equiv vp - D\partial p/\partial x$, p is probabilistic presence of the REV and J is the current. The velocity v is the overall drift constant velocity which is the terminal velocity, *i.e.* the constant velocity resulting from the competition between the driven force (the gradient of the global potential) and friction due to viscosity. It can be computed integrating the Hagen-Poiseuille equation on the network

$$nv = -\sigma \Delta P / L, \tag{2.18}$$

with $v = Q/A$, L, n and σ, respectively, the linear size, the density and the conductivity of the medium.

Let's study the stationary form of the Equation 2.17, *i.e.* $\partial p/\partial t = 0$:

$$\frac{\sigma \Delta P}{Ln} \frac{\partial p}{\partial x} + D \frac{\partial^2 p}{\partial x^2} = 0. \tag{2.19}$$

Thus, one solution of Equation 2.19 is given by

$$p(x) = \alpha \exp\left(-\sigma \Delta P x / nLD\right) + \beta,$$

with α and β being two constants. The imposed potential difference is zero for negative x since the water heigh difference is only maintained for $x > 0$. Therefore, $J(x)|_{x=0} = 0$ and hence, the probability p is given by

$$p(x) \propto \exp\left(-\sigma \Delta P x / nLD\right) \tag{2.20}$$

On the other hand, the probability p can be computed using statistical mechanics. In addition to a potential given by $V(x) = \Delta P x/L$, each REV, located at x, experiences a random force from its surrounding (due to the motion of the other REVs). It is natural to assume that the overall system is in thermal equilibrium with the medium (the network). Thus, the system can be view as embedded in a thermal bath of temperature T. Such kind of systems at equilibrium are studied via the canonical ensemble and are described by the Boltzmann distribution. At equilibrium, we have

$$p(x) \propto \exp\left(-\Delta P x / LT\right) \tag{2.21}$$

Finally, given Equations (2.20) and (2.21), we obtain the Einstein relation

$$\sigma \propto nD \tag{2.22}$$

The Einstein relation is a result of the Fluctuation Dissipation Theorem (see for example [Täuber [2014]]). This theorem is interpreted in the following way. An REV flowing in a dense network experiences friction due to the viscosity and thus dissipates kinetic energy into thermal energy. Therefore, the motion of the REV experience thermal fluctuations. Imagine that the overall external potential (the pressure difference) is turned off. Thus, there is no more external force that moves the REV. However, it moves quickly around its initial positions due to collision with others REV (more precisely molecules fluctuates due to temperature and induce a movement on molecules of the REV). The thermal fluctuation is therefore converted in kinetic movement.

Fractal media and the Einstein relation.

The derivation of the Einstein relation does not rely on any assumption on the nature of the medium and also holds for fractal media. The validity of this relation is not guaranteed for real world systems such disordered media, see for example [Haynes and Roberts [2009]].

If L denotes the spatial length scale and d the dimension of the embedding space, the density n of a fractal object follows the relation $n \propto L^{d_f - d}$. The diffusion constant D depends also on the length L of a walk of duration t and is such that $D \equiv \frac{\langle r^2(t) \rangle}{t} \approx \frac{L^2}{t}$. Diffusion is characterized by the walk exponent d_w, and relates the mean square displacement $\langle r^2(t) \rangle$ of a random walker with the displacement time t and position $r(t)$ (see Equation 2.10):

$$\langle r^2(t) \rangle \propto t^{2/d_w}. \tag{2.23}$$

Therefore, assuming Equation 2.22, and the scaling law $\sigma \propto L^{-\tilde{\mu}}$, we obtain

$$\tilde{\mu} = -2 + d - d_f + d_w \tag{2.24}$$

Henceforth, we will refer to Equation (2.22) as the Einstein relation.

By definition of the resistance R and the conductivity σ we have,

$$\sigma \propto \frac{L^{2-d}}{R} = L^{2-d-\tilde{\zeta}}. \tag{2.25}$$

where d is the dimension of the embedding system (the cross section is L^{d-1} since in higher dimension than 3 it is a $d-1$ dimensional object). Therefore $\tilde{\mu} = -2 + d + \tilde{\zeta}$, and for $d = 2$ we have $\tilde{\mu} = \tilde{\zeta}$.

2.3.2 Random Fractals

Fractal behaviour can also be observed in a statistical way. This occurs when we study real world structures such as river networks, cost lines and surface of human brains. In this Section,

we introduce one of the simplest and most instructive model of random fractal which is called the **percolation model**.

The percolation model

Percolation is an outstanding model for disordered systems, for a complete introduction refer to Stauffer and Aharony [1994]. It is one of the simplest model of phase transition which is of primary importance in the study of fractal structure. Moreover, percolation is a natural way to study connectivity properties of clusters.

Let's work on an infinite 2 dimensional square lattice. Nodes of the lattice are randomly occupied with probability p and empty with probability $1 - p$. A set of occipied site that are first nearest neighbours is called a cluster. For small p the lattice is covered by isolated clusters. As p increases, the size of largest clusters grows. For a particular value of p, named the threshold probability p_c an infinite cluster spans the lattice and is surrounded by isolated finite size cluster (Figure 2.10). The typical linear size of clusters ξ (the correlation length, illustrated in Figure 2.11) diverges at $p = p_c$ and is given by

$$\xi \propto |p - p_c|^{-\nu} . \tag{2.26}$$

For $p > p_c$, ξ represents the typical size of the holes (Figure 2.10). The threshold probability depends on the lattice geometry. For a square lattice, for example, it is given by $p_c \approx 0.593$. Meanwhile, the exponent ν depends only on the lattice spatial dimension d and is said to be universal ($\nu = 4/3$, in 2 dimension for any lattice geometry).

The probability P_∞ that a node belongs to the infinite spanning cluster (in practice, the probability to belong to a cluster connecting borders of the considered domain) is zero for $p < p_c$. Close to and above p_c we have

$$P_\infty \propto (p - p_c)^\beta, \tag{2.27}$$

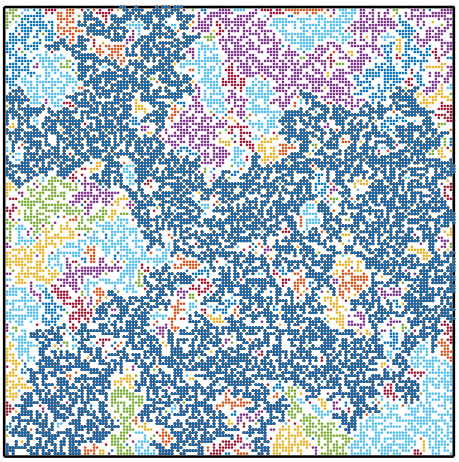

Figure 2.10: The percolation model on a 150×150 squares latice at $p = p_c \approx 0.593$.

with $\beta = 5/36$ denotes an other universal exponent for $d = 2$. The probability P_∞ is named the **order parameter** of the system. The system undergoes a phase transition (from a disconnected to connected state). One of the strengths of this model relies on the fact that, although being purely geometric, it reproduces all the essence of continuous phase transition (such, for example, the ferromagnetic transition exposed in Chapter 1). Percolation model define another universality class, different from the Ising model.

The divergence of the correlation length implies correlation (a collective behaviour) between nodes on all length scales. Thus, observed structures are self-similar. It is true even away from p_c, however self-similarity is observed up to a length scale of the order of ξ.

The fractal dimension of a percolation cluster, up to ξ, is known in two dimensions and is $d_f = 91/48 \approx 1.896$ (Stauffer and Aharony [1994]). However, the walk exponent and the conductivity exponent are only known trough numerical experiments or can be approximated by sophisticated calculus [Stenull and Janssen [2001]]. Reported exponents from the liter-

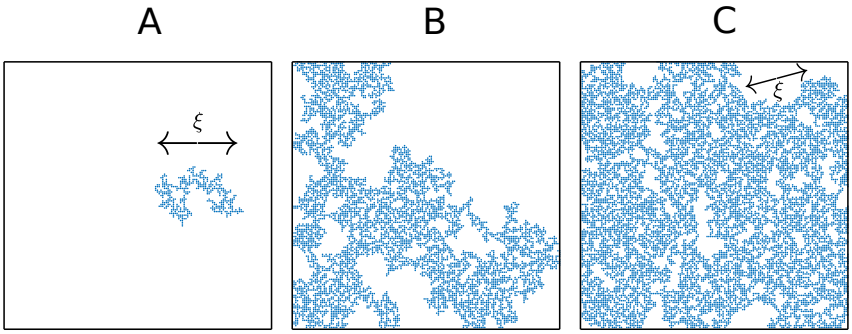

Figure 2.11: Largest clusters: (A) below p_c, (B) at p_c and (C) above p_c. (B) Notice, at $p = p_c$, ξ diverges, here, $\xi \sim L$, with L the linear size of the finite lattice on which we generate percolation clusters.

ature [Ben-Avraham and Havlin [2000]] are $d_w = 2.878 \pm 0.001$ and $\tilde{\mu} = 0.9826 \pm 0.0008$. Thus, meanwhile considering a random fractal structure, the 2-dimensional Einstein relation $\tilde{\mu} = -d_f + d_w$ is satisfied.

2.4 How to model karst networks as a system exhibiting scale invariances?

First, our aim is to characterize Tulum's karst networks as fractal objects. Therefore, in Chapter 3 and 4, we study their fractal dimensions together with their walk and conductivity behaviours. We will show that the networks are well defined as fractal structures. Moreover, we notice that the different karst networks are similar in terms of fractal dimension as well as for walk and conductivity exponents. Therefore, they can be modelled as the same random fractal.

In Chapter 5 we aim to built a model for karst networks that reproduces observed exponents. Make a purely geometrical model of karst networks, such as the iterative construction of the

Sierpinki gasket, would be poor in physical interpretations. We follow another way.

Fractal structures are systems exhibiting properties correlated on all length scales. This kind of collective behaviour is observed in a system that undergoes a continuous phase transition. Indeed, the correlation length of the system diverges at the phase transition. A karst network is a connected structure that transports water from inlets to outlets. Thus, a natural choice of order parameter is P_∞ being the probability that a node belongs to a network connecting the inlets and outlets. Therefore, we consider percolation networks. Percolation networks at p_c contain holes of all sizes, which is an interesting feature since karst networks present numerous flow path loops of various extensions (Figures 2.1 and 2.4). Therefore, our model relies on the percolation theory.

This kind of model (based on continuous phase transition) depends on a fine tuning to drive the network towards a critical point. However, as already mention in Chapter 1, it is expected that the scaling laws, describing emergent structure in nature, are generics. For example, river networks are modeled using the concept of Self-Organized Criticality [Rodríguez-Iturbe and Rinaldo [2001]] which is a model exhibiting generic scaling behaviours. An other example is landscape erosion [Pastor-Satorras and Rothman [1998]] which is described by a stochastic partial differential equation (similar to the Kardar-Parizi-Zhang equation [Kardar et al. [1986]]) that evolves in a generic way to scaling behaviours.

Although inspired by phase continuous transition, we suggest that the fine tuning of the parameters of our karst networks model is not completely arbitrary but is related to a minimization argument.

Chapter 3

Fractal dimension, walk dimension and conductivity exponent of karst networks around Tulum

Adapted from Hendrick, M., & Renard, P. (2016). *Fractal dimension, walk dimension and conductivity exponent of karst networks around Tulum.* Frontiers in Physics, 4, 27.

Abstract

Understanding the complex structure of karst networks is a challenge. In this work, we characterize the fractal properties of some of the largest coastal karst network systems in the world. They are located near the town of Tulum (Quintana Roo, Mexico). Their fractal dimension d_f, conductivity exponent $\tilde{\mu}$ and walk dimension d_w are estimated using real space renormalization and numerical simulations. We obtain the following values for these exponents: $d_f \approx 1.5$, $d_w \approx 2.4$, $\tilde{\mu} \approx 0.9$. We observe that the Einstein relation holds for

these structures $\tilde{\mu} \approx -d_f + d_w$. These results indicate that coastal karst networks can be considered as critical systems and this provides some foundations to model them within this framework.

3.1 Introduction

Karst network structures are still poorly understood because of the lack of a general framework to study them [Hartmann et al. [2014]], even if modeling and characterizing karst networks has been a long standing research topic [Kiraly [1975], Cornaton and Perrochet [2002], Hill et al. [2010], Jourde et al. [2002], Borghi et al. [2012]].

It is estimated that karst features cover 20 % of the globe's land surface [Ford and Williams [2013]]. Therefore understanding karst structures is crucial for many practical purposes, from pollution issues to ground stability assessment. Karst networks result from the dissolution of rocks by water through chemical reactions [Lace and Mylroie [2013]]. Dissolution leads to the creation of complex connected structures (from small conduits to caverns) where water flows and encounters less resistance due to friction than in porous or fractured rocks.

In this paper, we focus on the analysis of karst networks located around the town of Tulum (Quintana Roo, Mexico). They are natural, underground, coastal, networks transporting water from inland to the sea. The area of Tulum hosts two of the largest water filled networks in the world: Ox Bel Ha and Sac Actun (above 200 km of connected conduits for each one [Kambesis and Coke IV [2013]]). Due to their large sizes and the relatively simple and homogeneous geology (horizontal carbonate platform) of the underground, we expect that these networks exhibit a well marked statistical signature characterizing the physical processes of their formation.

We analyze these networks (mapped by cave-divers) as spatially embedded graphs. The large horizontal extension (about 10 km) compared to their vertical extent (around 12m) allows

us study these systems as embedded structure in plan view. Figure 3.1 shows Ox Bel Ha and Sac Actun (proportionally rescaled such that the maximal vertical extension is 1). Water flows from the upstream part (top of Figure 3.1) to the sea (bottom of the Figure).

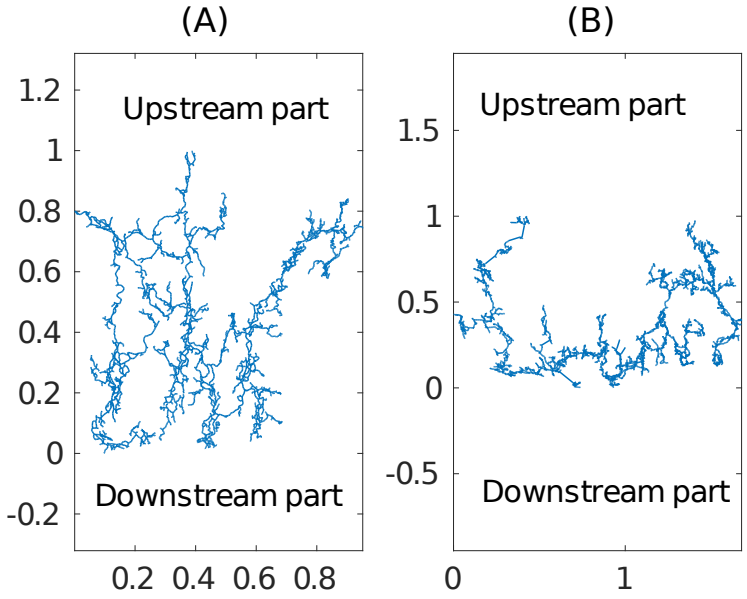

Figure 3.1: Cave divers's maps of (A) the Ox Bel Ha system and (B) Sac Actun.

In this paper, we propose a method to characterize karst systems using statistical mechanics tools and show that they exhibit fractal properties. We use the Song, Havlin and Makse (SHM) renormalization scheme [Song et al. [2005]] to the study these networks. To our knowledge, this is the first application of the SHM renormalization scheme to compute the fractal dimension of spatially embedded networks. We then analyze the network transport properties in terms of diffusion (random walk simulation) and conductivity (solving Kirchhoff equations).

Fractal concepts are not new to karst systems, with previous studies characterizing karst structures as fractal objects. However, these studies were limited to estimating fractal dimensions of relatively small networks (1-10 km of connected conduits [Laverty [1987], Kusumayudha et al. [2000], Jeannin et al. [2007], Pardo-Iguzquiza et al. [2011])]. Reported fractal dimension range from 1.043 to 1.67. However, a clear, physically based overall picture is still missing, with no attention paid to the study of transport properties (conductivity and diffusion) that complete the characterization of karst networks as 'standard' fractal structures.

We show through numerical experiments that the conductivity scales as a power law of the Euclidean distance between two points of the network for both Ox Bel Ha and Sac Actun. The two networks share a similar structure, in terms of fractal dimension d_f, random walk exponent d_w and conductivity exponent $\tilde{\mu}$. This is not surprising as they result from the same physical process in the same environment. The Einstein relation $\tilde{\mu} = -2 + d - d_f + d_w$ (we work in 2 dimensions, $d = 2$) holds in the 95% confidence intervals, and notice that $\tilde{\mu}$ is quite robust through renormalization. These results highlight the deep fractal nature of karst network around Tulum.

The structure of the paper is as follows. Section 2 presents the study of the fractal dimension of Tulum's karst networks and the network renormalization scheme. Section 3 describes the determination of the value of the conductivity exponent using Einstein relation and the numerically computed walk exponent for both networks. Section 4 investigates the validity of the scaling law hypothesis for conductivity and the Einstein relation. We finish with a discussion and perspectives for future work.

3.2 Fractal dimension of Ox Bel Ha and Sac Actun

To apply standard box counting algorithms on a network, it is first necessary to convert it to a binary image. However, significant information about network's topology may be lost during this conversion, resulting in coarse-grained images of the network and lost connectivity information of the underlying structure. In this paper, we employ a different approach.

Ox Bel Ha and Sac Actun networks are planar spatial graphs. Distributions of link lengths[1] and node degrees are narrow for both networks, see Figure 3.2. Thus, in terms of degree distribution and links sizes both networks are quite homogeneous. Some basic properties of these networks are listed on Table 3.1.

Table 3.1: Basic networks properties for Ox Bel Ha and Sac Actun rescaled such that the maximal vertical extension is 1. N, l, L, λ and $\bar{k}$ are, repsectively, the number of nodes, the number of links, the sum of links length, the mean links size and the mean node degree. Notice that $\lambda \approx L/l$.

	N	l	L	λ	$\bar{k}$
Ox Bel Ha	19016	21478	31	$1.4\ 10^{-3}$	2.26
Sac Actun	30200	35974	26	$7.46\ 10^{-4}$	2.4

We apply the renormalization procedure proposed by Song, Havlin and Makse in [Song et al. [2005]] to compute the fractal dimension of Ox Bel Ha and Sac Actun networks. Especially, we employ the Maximun-Excluded-Mass-Burning version of the scheme [Song et al. [2007]], which is adapted to the study of homogeneous networks. The procedure is illustrated in Figure

[1] A link does not represent a conduits but rather is the path between two sampled points in the network (a conduit can be mapped with N points and hence is represented by $N-1$ links).

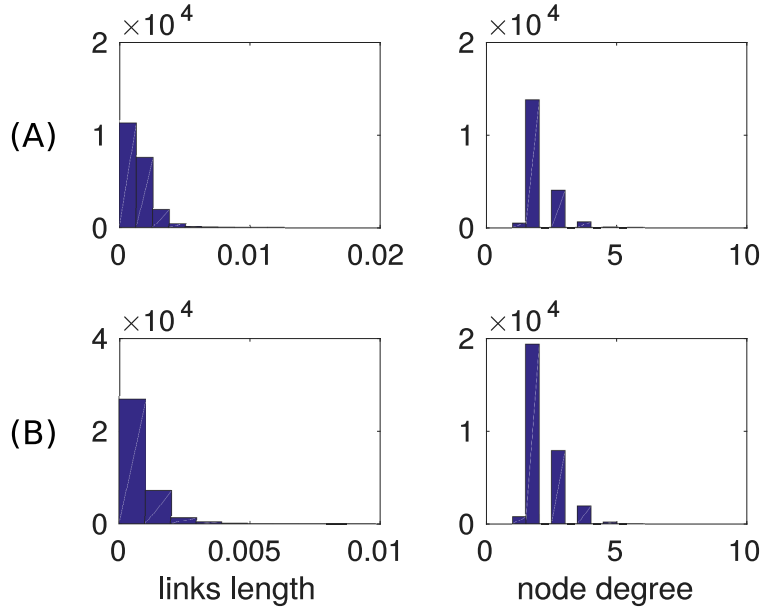

Figure 3.2: Links lengths size distribution and node degree distribution. Line (A) Ox Bel Ha, line (B) Sac Actun. Links length is computed on rescaled network hence it is a renormlized length.

3.3. The network is tiled with boxes. A box is centred on a node of the network and contains all neighbouring nodes separated, from the center, by a maximal chemical (topological) distance less than l_B (the chemical distance between two nodes is the minimum number of links needed to go from one node to the other one). The parameter l_B is named the box size. To build the renormalized network, each box is replaced by a single node. Two renormalized nodes (a and b) are linked if a link is connecting at least one node belonging to the box corresponding to a with one node of the box corresponding to b in the original network.

As we are dealing with spatial networks, a box (renormalized node) is located at the mean position of nodes that constitute it. At each renormalization step, we compute the mean of the distribution of link lengths and we take this as the characteristic

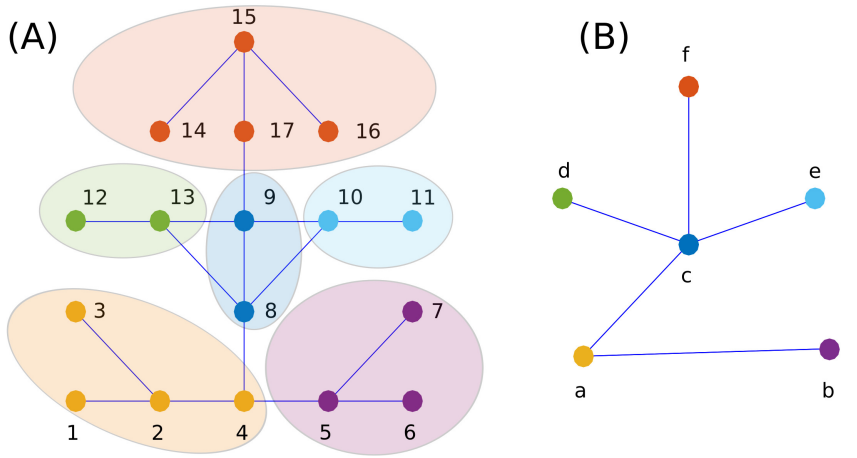

Figure 3.3: SHM renormalization scheme (the Maximun-Excluded-Mass-Burning version) illustrated on a generic network for a box of size $l_B = 2$. (A) the initial network and (B) the first renormalization step. For example, on (A) renormalization of the yellow box (centred on the node 2) gives on (B) the yellow node labelled by a. The renormalized node, a, is located at the barycenter of the parents nodes 1,2,3 and 4. The procedure is repeated until the network collapse into an unique node. We can notice that the mean of links sizes grows from (A) to (B).

length scale λ of the network. We notice that

$$N(G_\lambda) \propto \lambda^{-d_f}, \tag{3.1}$$

where N is the number of nodes needed to tile the network G_λ and d_f is its fractal dimension. As l_B has no physical significance in our study (due to cave divers mapping procedure), we take λ as the relevant length scale.

To illustrate the procedure, consider, as an example, the iterative building process of the 2 dimensional Sierpinski gasket as an inverse renormalization process (Figure 3.4). The number of nodes $N(t)$ (*i.e.* the number of vertices) at the building step t is $N(t) = 3(3^t + 1)/2$. Meanwhile, the links length $\lambda(t)$ (the

edge length) is reduced (compared to the $t-1$ step) by a factor 2^t. Therefore, assuming Equation (3.1) and $t \gg 1$ we have,

$$d_f \approx \frac{(t+1)\log 3}{t \log 2} \approx \frac{\log 3}{\log 2} \tag{3.2}$$

which is the well known Sierpinski gasket fractal dimension in 2 dimensions.

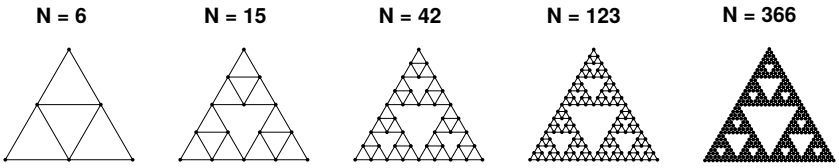

Figure 3.4: Sierpinski gasket and the corresponding number of nodes.

Figure 3.5 shows that the SHM renormalization scheme applied to spatially embedded planar networks succeeds (in the 95 % confidence interval) to estimate the dimension of well known fractal structures such as diffusion limited aggregate, percolation cluster and random space filling lattice. Computed fractal dimensions and reference values from [Ben-Avraham and Havlin [2000]] are presented in Table 3.2. This gives us confidence on the relevance of the computed dimension for Ox Bel Ha and Sac Actun networks.

Figure 3.6 illustrates four steps of the renormalization procedure applied to Ox Bel Ha. The renormalization scheme allows studying the large scale behaviour of the network and how it evolves with scale. This procedure reveals the main structure of the network (analogous to its skeleton). One observes for example, in Figure 3.6 how large loops and main paths are highlighted.

Figures 3.7(A) and 3.7(B) show the results of the application of this procedure for the computation of the fractal dimensions for Ox Bel Ha and Sac Actun. Fractal dimensions of the two

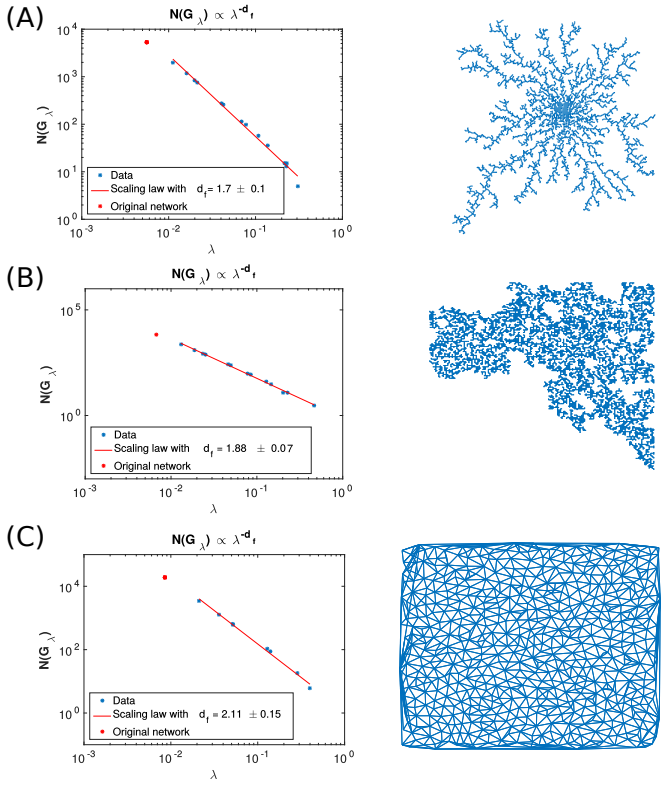

Figure 3.5: Fractal dimension computed through renormalization for (A) DLA, (B) percolated cluster and (C) space filling networks.

networks are quite close (considering the 95 % confidence interval) and are around $d_f \approx 1.5$. It is not surprising that these two networks are characterized by almost the same fractal dimension since they formed from the same physical processes, acting in the same environment at the same time.

Table 3.2: d_f are fractal dimensions computed with the SHM's scheme (the estimated errors correspond the 95 % confidence intervals). d_f^{ref} are reference values from Ben-Avraham and Havlin [2000]

	d_f	d_f^{ref}
DLA	1.7 ± 0.1	1.71 ± 0.07
Percolating cluster	1.88 ± 0.07	$91/48 \approx 1.896$
Space filling network	2.11 ± 0.15	2

3.3 Conductivity exponent for Ox Bel Ha and Sac Actun

The results of the previous Section encourage further exploration of the fractal properties of Tulum's karst networks. It is well known, see [Ben-Avraham and Havlin [2000]], that the conductivity σ between two points of a fractal structure (*e.g.* a percolating cluster) follows a scaling law. The conductivity σ is a function of the Euclidean distance between these two points

$$\sigma(L) \propto L^{-\tilde{\mu}} \tag{3.3}$$

with $\tilde{\mu}$ the conductivity exponent, $L = \|x - x'\|$, x, x' the location of two nodes of the network, and $\|\cdot\|$ the Euclidean distance. The conductivity exponent can be related to the structural properties of the fractal object (its fractal dimension and walk exponent) using the Einstein relation.

The Einstein relation links the conductivity to the diffusion coefficient D and the density n of the substrate (see again [Ben-Avraham and Havlin [2000]])

$$\sigma \propto nD \tag{3.4}$$

Here, the substrate is the network which is embedded in the plane. Therefore, n depends on the spatial length scale L through

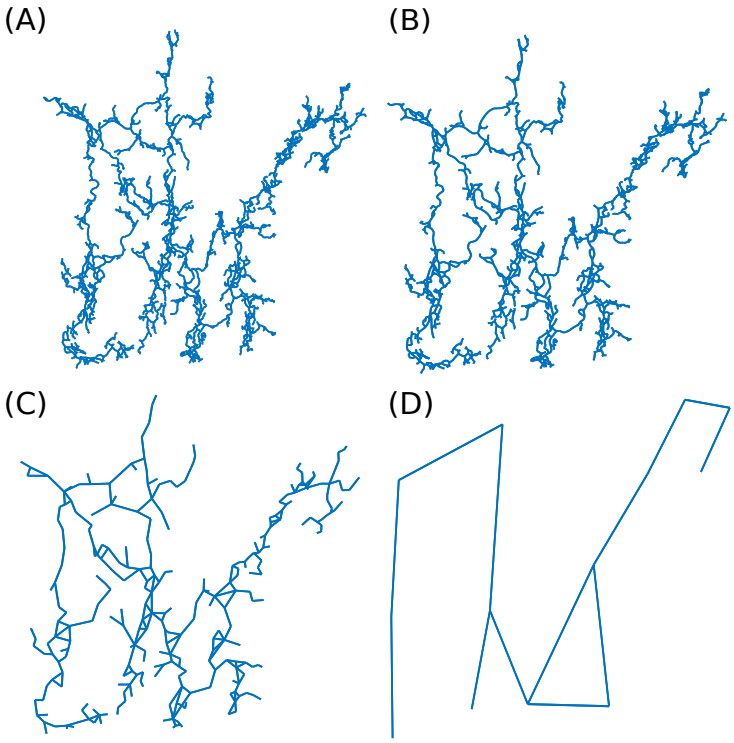

Figure 3.6: Renormalization scheme applied to Ox Bel Ha for $l_B = 2$. (A) original network, (B), (C), (D) renormalized network after 2,4 and 7 iterations.

the relation $n \propto L^{d_f - d}$, with $d = 2$. The diffusion constant depends also on the length L of a walk of duration t and is $D \equiv \frac{\langle r^2(t) \rangle}{t} \approx \frac{L^2}{t}$. Diffusion is characterized by the walk exponent d_w, and relates the mean square displacement $\langle r^2(t) \rangle$ of a random walker with the displacement time t and position $r(t)$:

$$\langle r^2(t) \rangle \propto t^{2/d_w} \tag{3.5}$$

with $\langle r^2(t) \rangle = \frac{1}{t} \sum_{i=0}^{t} \|r(i) - \bar{r}\|^2$ and $\bar{r}$ is the time averaged position of the walker.

Therefore, assuming Equation 3.4, we have the conductivity

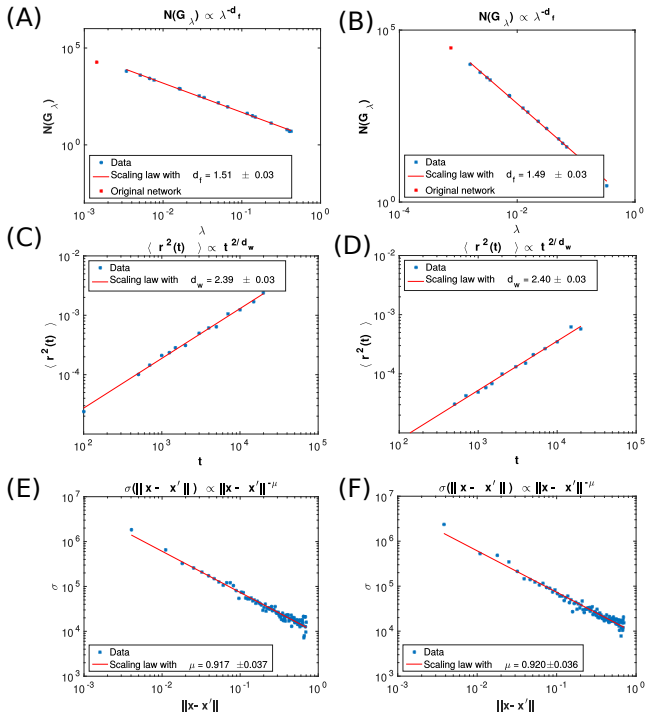

Figure 3.7: Numerical results for Ox Bel and Sac Actun respectively on the left column and on the right column. (A), (B): fractal exponents. (C), (D): walk exponents. (E), (F): conductivity exponents. The estimated errors correspond the 95 % confidence intervals for the fitted scaling laws.

exponent $\tilde{\mu}_E$

$$\tilde{\mu}_E = -2 + d - d_f + d_w \tag{3.6}$$

with

- d the dimension of the embedding space
- d_f the fractal dimension
- d_w the random walk exponent

We compute d_w on Ox Bel Ha and Sac Actun through random walk simulations. A random walk of t steps on a network is simply simulated taking a node randomly as the origin of the walk. From the origin the walker moves to one of its connected neighbours. The walk is stopped after t steps. Results are reported in Figure 3.7. Assuming Equation (3.6) we are able to compute the conductivity exponent $\tilde{\mu}_E$ for Ox Bel Ha and Sac Actun, results are reported on the last column of Table 3.3.

Table 3.3: Fractal dimension d_f, walk exponent d_w, conductivity exponent $\tilde{\mu}$, and the conductivity exponent $\tilde{\mu}_E = d_f + d_w$ given by Equation 3.6 for Ox Bel Ha (OBH) and Sac Actun (SA).

	d_f	d_w	$\tilde{\mu}$	$\tilde{\mu}_E$
OBH	1.51 ± 0.03	2.39 ± 0.03	0.917 ± 0.037	0.88 ± 0.04
SA	1.49 ± 0.03	2.40 ± 0.03	0.920 ± 0.036	0.91 ± 0.05

3.4 Flow simulation and the validity of the Einstein relation

To examine the validity of Equation (3.6) for karst networks, we numerically investigate how the conductivity behaves between two randomly sampled nodes, A and B. Thus, we solve Kirchhoff equations [Strang [1988]] for Hagen-Poiseuille flow (or equivalently for a linear Ohm law) for the sub-network connecting A to B by imposing the inflow rate (we impose the same inflow rate for each sampled sub-network).

As we have no accurate information about the distribution of conduits radii (except a lower cut off, around 1 meter, due to the finite size of cave divers that mapped the network) we take it as unity. Hence the resistance of a link depends only of its length (which is peaked around λ).

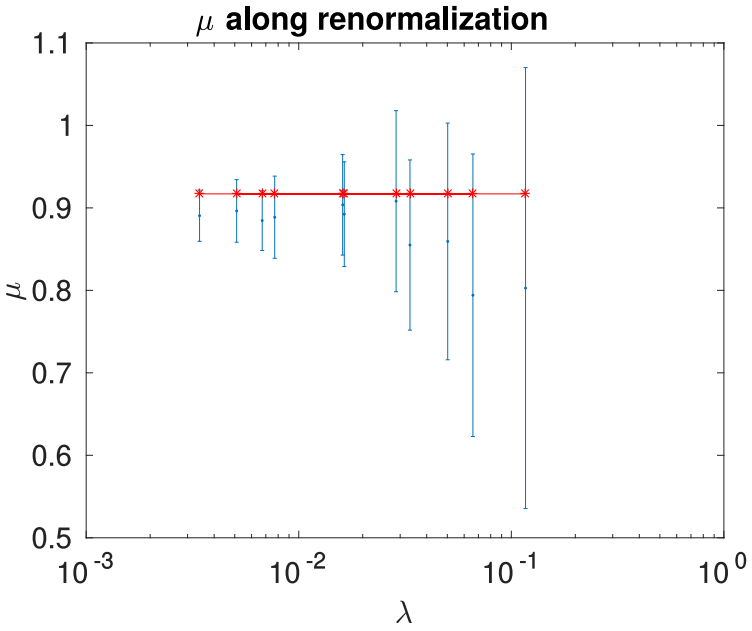

Figure 3.8: Conductivity exponent computed for Ox Bel Ha and its renormalizations at characteristic length scale λ. The line is the conductivity exponent of the original network.

Figure 3.7 shows plots of the conductivity with respect to the Euclidean distance and the value of the computed conductivity exponent are reported in Table 3.3. It is worth noticing that Einstein relation holds (in the 95% confidence interval) for karst networks around Tulum. It is not surprising as Ox Bel Ha and Sac Actun networks exhibit well marked fractal features. Moreover, the conductivity exponent seems to be invariant under renormalization for small characteristic length scales λ. At large scale, the value and the uncertainty on $\tilde{\mu}$ is larger. Figure 3.8 shows results of the computation of the conductivity exponent at different renormalization steps of Ox Bel Ha (a similar result holds for Sac Actun). This observation gives us confidence for modelling karst networks as a systems near criticality [Täuber [2014]].

3.5 Discussion

This study highlights the fractal properties of the karst networks around Tulum, Mexico. They behave as fractal structures. Networks are characterized by a scaling law for conductivity and anomalous diffusion. The Einstein relation holds for these structures.

We expect that these networks are not unique. Other coastal systems in the world, such as the ones encountered in Florida or in the Bahamas, are suspected to exhibit similar structures since they developed in geological and climatic environments (limestone platforms in a tropical and coastal area) similar to Tulum's karst networks.

Further analysis using data from such sites should be conducted to test our numerical results. Additional investigations (theoretical and numerical) should also conducted to determine the influence of turbulent flow on the conductivity exponent, and on the scaling hypothesis, because water flow in karst systems often occurs at high Reynolds number.

Our results indicate that the coastal karst networks of Tulum behave as self-similar structures, with well-behaved scaling properties. This suggests that karst systems can be studied and modeled in the framework of critical phenomena. Such models should be able to reproduce observed exponents and help explain the underlying process that results in the emergence of those values.

Chapter 4

Properties of small karst networks located around the town of Tulum

4.1 Introduction

In Chapter 3, we analysed the fractal properties of the two largest karst networks located in the area of Tulum (Quintana Roo, Mexico), the Sac Actun and Ox Bel Ha systems. Both, are characterized by a fractal dimension $d_f \approx 1.5$, a walk exponent $d_w \approx 2.4$ and a conductivity exponent $\tilde{\mu} \approx 0.9$. The Einstein relation $\tilde{\mu} = -d_f + d_w$ seems to hold for these structures.

The area of Tulum hosts other (smaller) karst networks (Figure 4.1). In this Chapter, we briefly discuss basic topological and geometrical properties of these networks and show results about the study of their fractal properties in comparison with Ox Bel Ha and Sac Actun networks. We also discuss about the total length of karst networks present over the state of Quintana Roo.

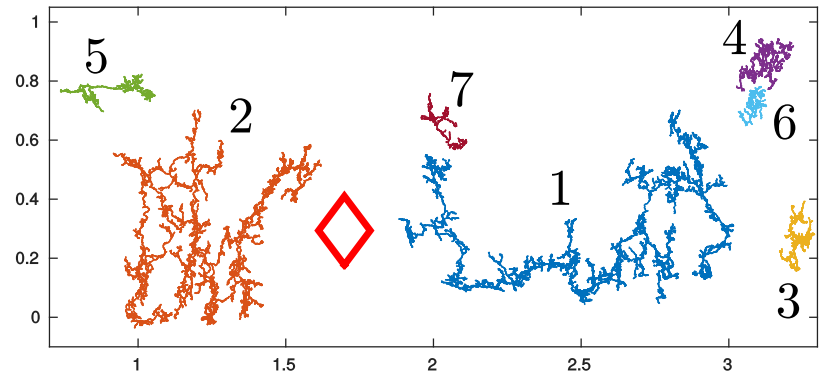

Figure 4.1: The town of Tulum (symbolized by the tick diamond) and the main surrounding karst networks

4.2 Topological, geometrical and fractal properties of Tulum's karst networks

In [Hendrick and Renard [2016]], we focus on the study of the two largest networks (about 200 km of conduits for each one) located in the vicinity of the town of Tulum because the aim was to characterized their structural and transport properties in a statistical way. However, the area of Tulum is highly karstified and smaller karst networks are located in this zone. Their sizes range from 15 km to 45 km of conduits (labelled 3 to 7 in Figure 4.1, labels 1 and 2 are respectively Sac Actun and Ox Bel Ha).

Basics networks properties are listed in Table 4.1. These networks are characterized by a degree distribution of mean $\bar{k} \approx 2.4$.

We study the ratio N/l with N the number of nodes and l the number of links. It is an indicator of the deviation of the structure from a tree structure and from a maximal planar graph. Indeed, a tree is a connected graph of N nodes and $N-1$ links (and hence a loopless network), thus, $N/l = N/(N-1)$ which is 1 in the limit of large N for a tree. A planar graph

is a structure drawable in the plane such that links intersect only at nodes. A planar graph is maximal if adding an other link it looses is planarity property. Planar maximal graphs are characterized by $l = 3N - 6$, thus the ratio $N/l \to 1/3$ for large N. Observed karst networks contains loops but stay close to a tree structure since they are characterized by a $N/l \approx 0.86$.

The distribution of links size is narrow (for each network). Therefore, the total networks length L (the sum of links length) is well approximated by $L \approx \lambda l$, with λ the mean of the distribution of links size. These results indicate us that the considered networks are quite homogeneous structures in terms of topology (narrow degree distribution) and geometry (narrow links size distribution). Based on these indicators, the networks look similar each other. Expect from the total length L, Sac Actun and Ox Bel Ha (networks labelled 1 and 2) are not distinguishable from the other networks.

Table 4.1: Basic propeties of karst networks around Tulum. The number of nodes and links are respectively noted N and l. The total links length L (*i.e.* the sum of links length) is computed in the rescaled frame of Figure 4.1. The mean links size is noted λ and the mean of node's degree is $\bar{k}$. Labels correspond to networks of Figure 4.1.

	N	l	N/l	L	λ ($[10^{-4}]$)	$l\lambda$	$\bar{k}$
1	30200	35974	0.84	26.9	7	25.2	2.40
2	19016	21478	0.89	21.8	10	21.5	2.26
3	4236	5174	0.82	3	6	3.1	2.45
4	3235	3888	0.83	3.7	9	3.5	2.44
5	2840	3316	0.86	2.4	7	2.3	2.34
6	1809	2089	0.87	1.5	7	1.46	2.30
7	1370	1630	0.84	1.6	10	1.63	2.37

Next, we focus on their fractal properties. We compute the fractal dimension d_f, walk exponent d_w and conductivity exponent $\tilde{\mu}$ of these networks (Table 4.2). All exponents deviates from those of Sac Actun and Ox Bel Ha. Except the network

Table 4.2: Fractal dimension d_f, walk exponent d_w and conductivty exponent $\tilde{\mu}$ of networks around Tulum. Labels correspond to networks of Figure 4.1 and $\tilde{\mu}_E = -d_f + d_w$ is given by the Einstein relation.

Label	d_f	d_w	$\tilde{\mu}$	$\tilde{\mu}_E$
1	1.49 ± 0.03	2.40 ± 0.03	0.920 ± 0.036	0.91 ± 0.05
2	1.51 ± 0.03	2.39 ± 0.03	0.917 ± 0.037	0.88 ± 0.04
3	1.57 ± 0.06	2.44 ± 0.04	0.875 ± 0.022	0.86 ± 0.07
4	1.58 ± 0.07	2.35 ± 0.03	0.983 ± 0.025	0.77 ± 0.07
5	1.42 ± 0.02	2.40 ± 0.04	1.036 ± 0.026	0.98 ± 0.04
6	1.65 ± 0.17	2.47 ± 0.03	0.957 ± 0.035	0.82 ± 0.17
7	1.46 ± 0.04	2.59 ± 0.05	0.919 ± 0.026	1.10 ± 0.06
(1–2)	1.50	2.40	0.92	0.90
(3–7)	1.54	2.45	0.95	0.91
(1–7)	1.53	2.43	0.94	0.90

5, the error interval associated to the fractal dimension is larger than our reference networks. The fractal dimension of the networks (3–7) overlap considering the errors interval with those of Ox Bel Ha and Sac Actun (except the network 5 which is significantly different). The walk exponent is rather the same for networks labelled from 1 to 5. The networks (6–7) are characterized by an higher d_w than the others in the set. In term of conductivity exponent networks (4–5) do not match with what we observe for Ox Bel Ha and Sac Actun. The Eintein relation is satisfied (in the interval errors which are quite large) for all networks expect networks 4 and 7.

To compare the results, we compute average values on the subsets of our set of data. The first subset (1–2), is our reference, the two largest networks, Sac Actun and Ox Bel Ha. The second subset (3–7), is made of the set of small networks which where not considered in Chapter 3. The last one is the complete set of data (1–7).

We observed that, in average, structure of smallest networks (3–7) is reasonably close to the reference set (1–2) with a signif-

icant deviation in term of d_w (considering the error intervals of the exponents of (1–2)). The properties of the entire set, (1–7) are in average close to (1–2).

These results comfort us that computed exponents are representative of the structure systems of this area. And thus, they may be useful to built a karst networks model.

4.3 Cumulative distribution function of the length of karst networks in the Quintana Roo state

The Quintana Roo Speleological Survey[1] lists 102 underwater karst networks, comprising more than 1.15 km of conduits, in the state of Quintana Roo.

We do not have maps of all these networks. However, the information about their total length is available. This list allows us to study karst network organization at a larger scale than the area of Tulum. We compute the probability distribution of the total length of all these karst networks. Thus we consider the complementary cumulative distribution function (ccdf) of networks length L. This ccdf is well fitted by a scaling law (Figure 4.2).

Therefore, self-similarity seems not be be restricted to intensive networks properties (*i.e.* properties which do not depend on the system size). The scaling behaviour of networks size suggest that, even at the scale of the Quintana Roo state, the karst networks behave as fractal structures. However, fractal dimension, walk and conductivity exponents may have a different origin than karst network length. The latter can be controlled by large scale geological constraints independently from the dissolution process.

It is important to notice that the ccdf may change in the future, since many effort are made by cave divers to connect

[1] https://caves.org/project/qrss/

systems. In the remainder of this thesis, we do not consider further the network length property and we focus on intensive aspects.

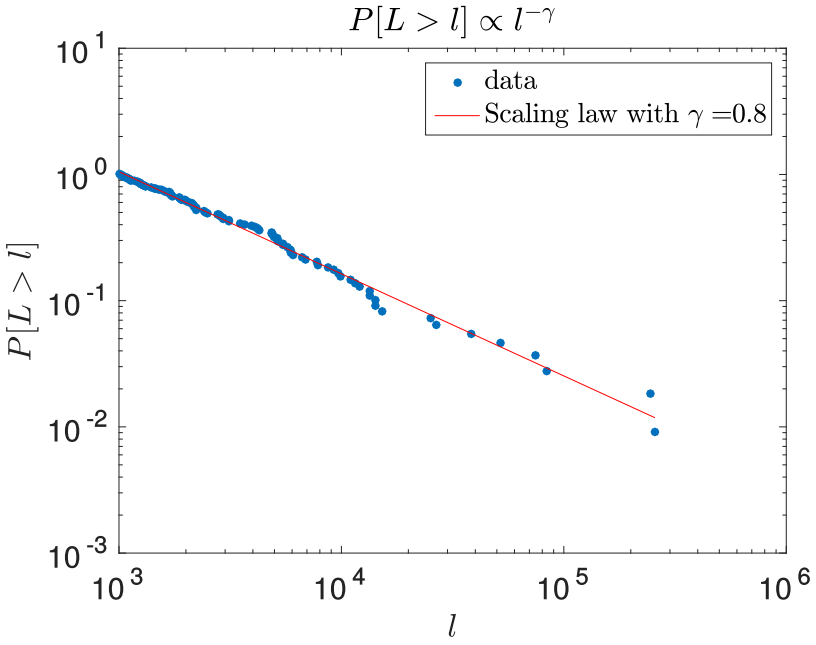

Figure 4.2: Complementary cumulative distribution function of networks length (in meters) located in the Quintana Roo state.

4.4 Conclusion

This Chapter helped to better characterize karst networks of the area of Tulum. The small networks (networks 3–7 in Figure 4.1) exhibit similar scaling behaviour than Sac Actun and Ox Bel Ha. It reinforces us to consider these exponents as representative of this type of karst networks and seems to be a proper way to characterize and study the underlying physics at the origin of the emergence of these networks.

All these karst networks can be viewed as part of a unique karst system due to their geographical proximity. It is expected

that, in a close future, connections between these systems will be found, however, conduit collapses could prevent them.

In the remainder of our work we take as reference networks Ox Bel Ha and Sac Actun since they are significantly larger than the other networks located in the vicinity of Tulum.

Chapter 5

Subnetworks of percolation backbones to model karst systems around Tulum, Mexico

Adapted from Hendrick M and Renard P (2016). *Subnetworks of percolation backbones to model karst systems around Tulum, Mexico.* Frontiers in Physics 4:43. doi: 10.3389/fphy.2016.00043

Abstract

Karstic caves, which play a key role in groundwater transport, are often organized as complex connected networks resulting from the dissolution of carbonate rocks. In this work, we propose a new model to describe and study the structures of the two largest submersed karst networks in the world. Both of these networks are located in the area of Tulum (Quintana Roo, Mexico). In a previous work Hendrick and Renard [2016] we showed that these networks behave as self-similar structures exhibiting well-defined scaling behaviours. In this paper, we suggest that these networks can be modeled using substructures of

percolation clusters (θ-subnetworks) having similar structural behaviour (in terms of fractal dimension and conductivity exponent) to those observed in Tulum's karst networks. We show in addition that these θ-subnetworks correspond to structures that minimise a global function, where this global function includes energy dissipation by the viscous forces when water flows through the network, and the cost of network formation itself.

5.1 Introduction

In a previous paper Hendrick and Renard [2016], we studied the fractal properties of the Ox Bel Ha and Sac Actun karstic networks in the region of Tulum, Mexico using real space renormalization and numerical simulations. We found that both networks have similar structures with well defined fractal dimension $d_f \approx 1.5$, conductivity exponent $\tilde{\mu} \approx 0.9$ and walk dimension $d_w \approx 2.4$. We also observed that these exponents are related by the Einstein relation.

Here we build on this work and propose a new model allowing the description of those systems, and study how their structures may emerge from general energy dissipation principles.

Previous authors have proposed several models for describing the geometry of karstic networks. The most comprehensive are based on a full mathematical description of the physical and chemical processes leading to the dissolution of carbonates (for example Groves and Howard [1994], Dreybrodt et al. [2002], Liedl et al. [2003]). They provide a detailed and deterministic description of the formation of underground cave networks and allow the time scales of these processes to be estimated. However, they require large, complex, and highly non-linear sets of partial differential equations to be solved. Simplifications and approximations of these processes were also proposed to enable the generation of stochastic networks that resemble actual networks Jaquet et al. [2004], Borghi et al. [2012], Collon-Drouaillet et al. [2012]. Even simpler models are based on the

statistical resampling of existing data sets and allow stochastic networks to be generated which reproduce the main statistical characteristics of the training networks Pardo-Iguzquiza et al. [2012]. Amongst these studies, Ronayne and Gorelick Ronayne and Gorelick [2006], Ronayne [2013] used the invasion percolation model of Stark Stark [1991] and investigated its large scale flow and transport properties. A weakness of these existing models is that they consider only networks having the structure of a tree, while our observations in Tulum show that the actual networks contain a significant amount of loops. Therefore there is a need for a model better suited to our case. Karst networks including numerous loops (called anastomotic structures Palmer [1991]), are also observed in other locations, thus requiring the investigation of improved models that include loops.

Many natural systems exhibit fractal properties and can be modeled as critical phenomena Sornette [2006] using different frameworks. For example, the structure of river basins can be analysed and modeled using self-organized criticality Rodríguez-Iturbe and Rinaldo [2001], landscape erosion was modeled considering a Kardar–Parisi–Zhang like equation Pastor-Satorras and Rothman [1998], or flow through porous media was described using the backbone of critical percolation clusters Stanley and Coniglio [1984].

Here we adopt the framework of percolation theory that is recognised as particularly well-suited to study connected structures Ben-Avraham and Havlin [2000], and conductivity and diffusion behaviour of percolation clusters are well known (random resistor network theory) Redner [2012]. We propose using subnetworks of percolation clusters, and show that these structures exhibit a similar fractal dimension, walk exponent and conductivity exponent to those observed. We also show how these subnetworks correspond to structures that minimize a function, where one term relates to energy dissipation from viscous flow and the other relates to the energy cost of creating the network. We discuss this minimization principle by analogy with dynamical models of river networks Rinaldo et al. [2006]

and early karst development Siemers and Dreybrodt [1998].

5.2 Materials and methods

5.2.1 Materials: The karst networks of Tulum

For clarity, we provide here a brief summary of previous findings Hendrick and Renard [2016].

The Ox Bel Ha and Sac Actun coastal karstic systems (Figure 5.1) are located around the city of Tulum (Quintana Roo, Mexico). They are the two largest submerged karst networks in the world. Each network is comprised of more than 200 km of connected conduits Kambesis and Coke IV [2013] and covers an area of about 10×10 km^2 with a limited vertical extension (average conduit depth is approximately 12 m). They formed within a horizontal layer of a relatively young carbonate platform and is relatively homogeneous in comparison to the network extension. These two remarkable properties (large extension and homogeneous geology) make these networks ideal for study. Due to the flat topography of the area, the hydraulic head gradient is small and ranges from 1 to 10 cm/km Bauer-Gottwein et al. [2011].

In Hendrick and Renard [2016], we analyzed these systems as spatial graphs embedded in the plane and characterized their properties. Figure 5.1 shows the maps of the two networks that were acquired by cave divers. A conduit is mapped as N points (nodes) linked by $N-1$ lines (links) in such a way that the degree of the inner nodes is 2 and, at the extremities where conduits meet, nodes are of degree greater than 2. Nodes located at dead ends of the networks have degree 1. The length of the links is roughly the size of the ruler used to map the network. These karst systems are quite homogeneous networks, characterized by a mean of degree distribution around 2.35 and a maximum node degree of 5.

Both Ox Bel Ha and Sac Actun have fractal dimension $d_f \approx$

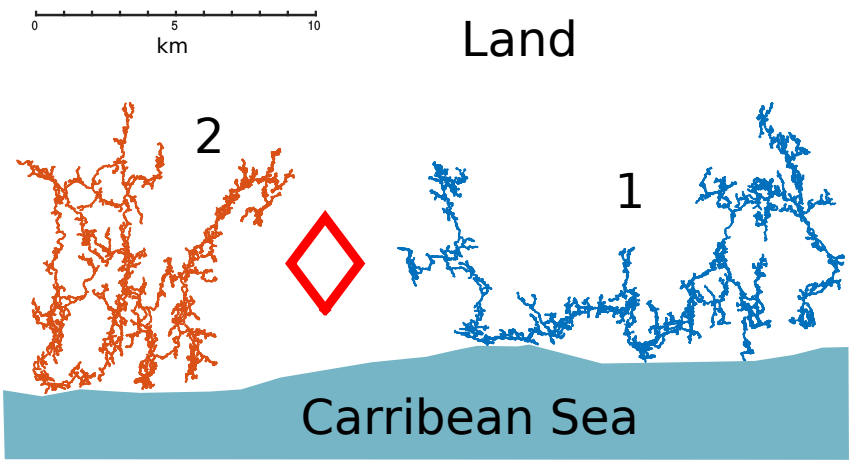

Figure 5.1: Cave divers' maps of (1) the Sac Actun system and (2) Ox Bel Ha. The diamond symbol represents the location of the town of Tulum and the coastline is sketched.

1.5, and exhibit the same conductivity scaling behaviour. For each network, the conductivity σ between two nodes scales with the Euclidean distance L that separates them, *i.e.* $\sigma(L) \propto L^{-\tilde{\mu}}$. Both networks are characterized by a conductivity exponent $\tilde{\mu} \approx 0.9$. They also share a similar diffusion behaviour. Diffusion is anomalous, the mean square displacement of a walker is given by $\langle r^2(t) \rangle \propto t^{2/d_w}$ with a walk exponent $d_w \approx 2.4$. It was also found that this set of exponents is in agreement with the (2-dimensional) Einstein relation $\tilde{\mu} = -d_f + d_w$.

5.2.2 Methods: computation of d_f, d_w and $\tilde{\mu}$

In the following, we study the fractal dimension, conductivity exponent and walk exponent of subnetworks of backbones using a large number of numerical simulations. The fractal dimension is computed using the Maximum-Excluded-Mass-Burning algorithm, described in Song et al. [2007]. Figure 5.2 illustrates one step during the renormalization procedure that is used to investigate the scaling properties of the networks. Details on

this procedure are provided in Hendrick and Renard [2016].

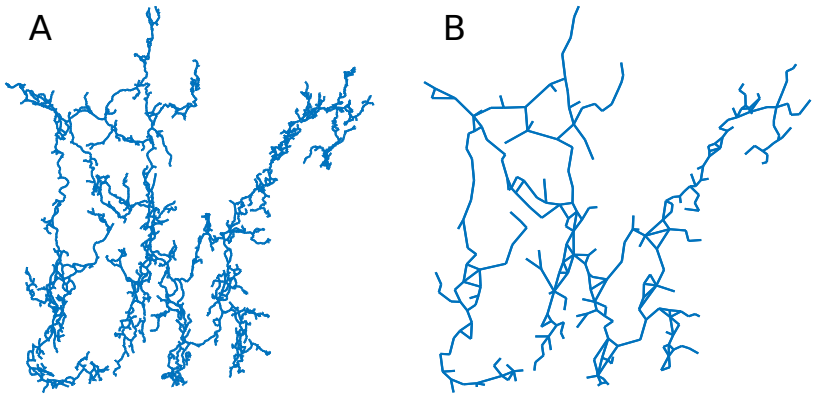

Figure 5.2: Renormalization of Ox Bel Ha using the Maximum-Excluded-Mass-Burning algorithm (Song et al. [2007]). Main orientation conduits are highlighted by renormalization. Main flow paths occurs from inland (upper part of the network) to the sea (bottom part).

The conductivity exponent is obtained evaluating the relation $\sigma(L) \propto L^{-\tilde{\mu}}$ for pairs of randomly sampled nodes (imposing for each sample pairs the same inflow rate). More precisely, we solve the Kirchhoff's circuit laws equations on the subnetwork connecting the two sampled nodes assuming, on each link, a flow described by the Hagen-Poiseuille law Strang [1988]. The resistance of each link is taken as unity (in the following, we work on square grids, thus link (conduit) length is fixed and we assume the same radius for each link). The walk exponent is computed by evaluating the mean square displacement of random walkers $\langle r^2(t) \rangle \propto t^{2/d_w}$ for different initial nodes.

5.3 Karst networks as subnetworks of the percolation backbone

5.3.1 Percolation theory: background considerations

The model is based on percolation theory that provides a standard framework for studying connected structures. The percolation model is that a fraction p of randomly chosen sites is occupied of a 2D square lattice. A cluster is a set of occupied sites connected to their nearest neighbours. When p is small, the clusters are isolated, while as p increases so do the size of the clusters. At the percolation threshold $p = p_c$ ($p_c \approx 0.593$ for a square lattice), a cluster spans the lattice (and would also span an infinite lattice). The correlation length ξ (the characteristic size of clusters) depends on p and diverges at $p = p_c$ as $\xi \sim |p - p_c|^{-\nu}$, with ν an universal exponent (independent of the lattice geometry) equal to 4/3 in two dimensions.

In our numerical simulations, the lattices are finite and the infinite cluster is defined as the largest cluster that connect the lattice's boundaries. We call this the the percolation cluster.

At criticality, *i.e.* at $p = p_c$, the percolation cluster is self-similar on all length scales (for an infinite lattice). Here we focus on the backbone of the percolation cluster, defined as the conducting part (*i.e.* links of the percolation cluster carrying non-zero flow rates) of the percolation cluster. The fractal dimension, walk exponent and conductivity exponent of the critical infinite percolation cluster and critical backbone are known Ben-Avraham and Havlin [2000]. Table 5.1 summarizes these values and compares them with the values measured for the karstic systems in Tulum. Since we observe quite different exponents we cannot simply use the percolation cluster or its backbone directly as a relevant model for karst networks.

The probability P_∞ that a node of a percolation cluster belongs to the infinite spanning cluster is zero for $p < p_c$ and is

Table 5.1: Fractal dimension d_f, conductivty exponent $\tilde{\mu}$ and walk exponent d_w of critical percolation cluster (cPC), critical backbone percolation cluster (cBB) and Tulum karst networks. Values for cPc and cBB come from (Ben-Avraham and Havlin [2000]), those of karst networks from (Hendrick and Renard [2016]). Conductivity exponents of cPc and cBB are the same since cBB is the conducting part of the cPc. Notice that away from p_c, percolation clusters are described by the same set of exponents up to ξ

	d_f	$\tilde{\mu}$	d_w
cPC	$91/48 \approx 1.896$	0.9826 ± 0.0008	2.878 ± 0.001
cBB	1.6432 ± 0.0008	0.9826 ± 0.0008	2.62 ± 0.03
Ox Bel Ha	1.51 ± 0.03	0.917 ± 0.037	2.39 ± 0.03
Sac Actun	1.49 ± 0.03	0.920 ± 0.036	2.40 ± 0.03

given by a power law $P_\infty \sim (p-p_c)^\beta$ close to and above p_c, with a universal exponent $\beta = 5/36$ in 2 dimensions. The percolation model is an archetype model for continuous phase transition. The probability P_∞ is the order parameter that distinguishes the disconnected phase to the connected phase. At the critical point $p = p_c$, a collective behaviour emerges at all length scales since the correlation length ξ diverges.

5.3.2 Proposed model using subnetwork of percolation backbone.

Karst networks are structures connecting inlets to outlets to allow the transport of water in heterogeneous media. Therefore, percolation theory is a natural starting point to model such of systems.

We consider networks in a busbar configuration where a fixed flux is prescribed between two parallel edges (Figure 5.3). We equally distribute the imposed total inflow rate between the nodes connected to the upstream edge. This geometry is adapted to the study of karst networks around Tulum since the

real networks transport groundwater from inland, where precipitation is recharging the system, toward the discharge area (the Caribbean Sea). The overall flux traversing the system is imposed by the climatic conditions. Thus, the total water flow rate traversing a karst network is time varying. We restrict our study to a prescribed fixed flux representing the average of the total flow rate over the year. We do not consider a fixed water height constraint. The sea level is a water head boundary. However, there is not an upstream structure, such as a lake, that may constitute a water height constraint for the networks of Tulum. Thus, we focus on systems experiencing a prescribed fixed flux.

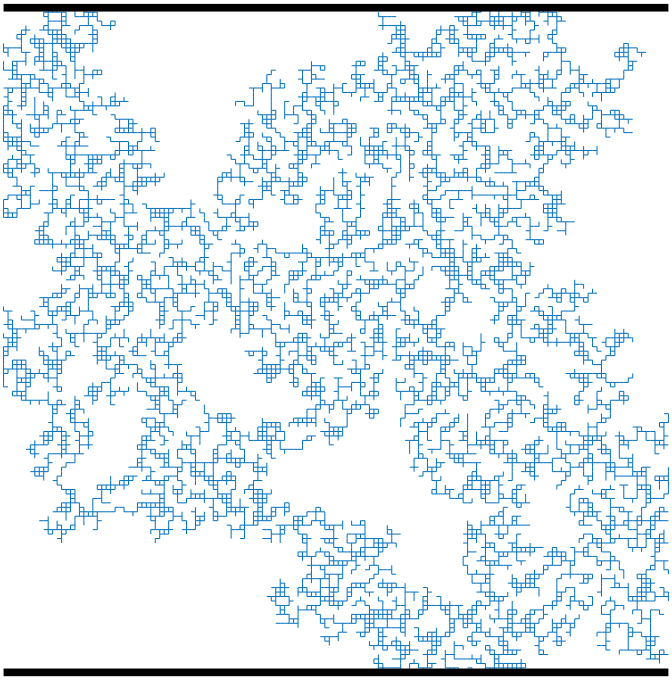

Figure 5.3: Illustration of the busbar geometry. A fixed flux is imposed between the two edges (represented by the black thick lines).

In the remainder of this work, we always consider the (largest)

percolation cluster that connects the two edges of the busbar configuration.

The proposed modeling procedure consists of numerically generating a percolation cluster for a given value of p (greater or equal to p_c). A prescribed flux is imposed on this network as a boundary condition between the edges of the busbar configuration. Water flows in the percolation cluster from the upstream edge to the downstream edge. The magnitude of the flow is computed by solving numerically Kirchhoff equation (using the Hagen-Poiseuille equation and a resistance of one for each link). It is then assumed that the karst network grows along the links of the percolation cluster that carry the strongest flow rates and that form a connected network that spans the two edges. Thus, we study karst networks as subnetworks of backbones of the percolation clusters.

We take as parameter $\theta = Q_t/Q_{\max}$ with Q_t the imposed threshold flow rate (*i.e.* minimal flow rate allowed for a link to be part of the karst network). $Q_{\max} = \max_{\langle i,j \rangle} \{Q_{ij}\}$ with $\langle i, j \rangle$ links of the percolation cluster and Q_{ij} the flow rate on the link $\langle i, j \rangle$[1]. The connected network of links carrying a flow rate above θ and which connect the two edges of the busbar geometry, are named θ-subnetwork. Examples of θ-subnetworks are illustrated in Figure 5.4.

5.3.3 Properties of θ-subnetworks

We investigate, through numerical simulations, the properties of θ-subnetworks for different site occupation probabilities at the critical point and above. We consider $p = 0.593$, 0.60, 0.61 and $p = 0.62$. For each probability, we generate 100 percolation clusters. From each percolation cluster, we extract[2] 6 θ-

[1]Indices i and j are labels of two linked nodes.

[2]The largest θ at which there exists a θ-subnetwork varies between percolation clusters. Therefore the interval of θ in which we sample the 6 θ-subnetworks differs from one percolation cluster to another. We do not sample at fixed θ's to avoid biased results or empty samples. Therefore, we

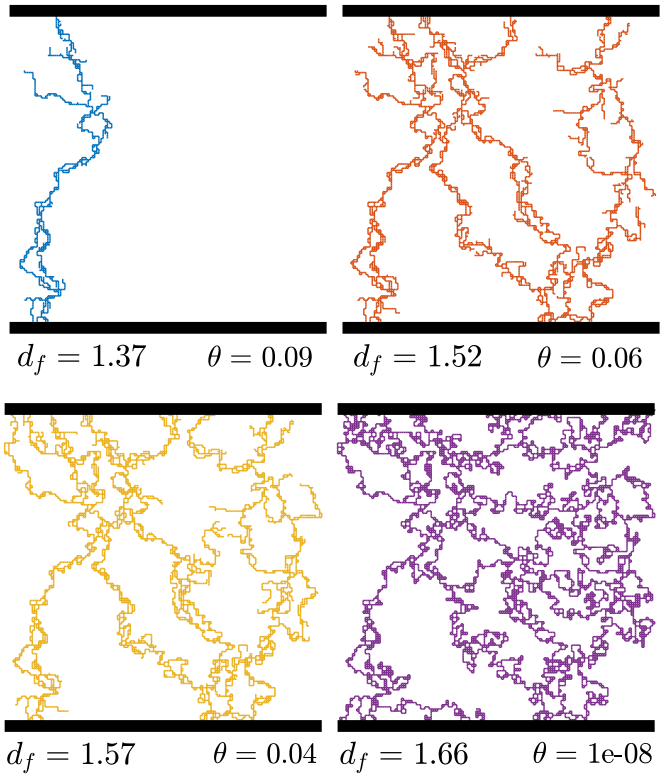

Figure 5.4: Illustration of θ-subnetworks extracted from a percolation cluster of site occupation probability $p = 0.60$. Notice that the size of largest loops grow from $\theta = 10^{-8}$ to $\theta = 0.06$ and then reduces.

subnetworks taking $\theta \in [0.01, 0.1]$. The effective fractal dimension, conductivity exponent and walk exponent are computed for each θ-subnetworks. The results of the numerical experiments are reported in Figure 5.5. The curves represent averages of all realizations for a given value of p. The percolation clusters are generated on a square lattice containing 150×150 nodes. We work with site percolation for computational convenience. The

extract 6 values of θ equally distributed on the interval $[0.01, \theta_{\max}]$, with $\theta_{\max}$ being the maximum value of θ for which a θ-subnetwork exists.

percolation network is built by creating links between first nearest neighbours (nodes separated by a maximal distance equal to the lattice parameters).

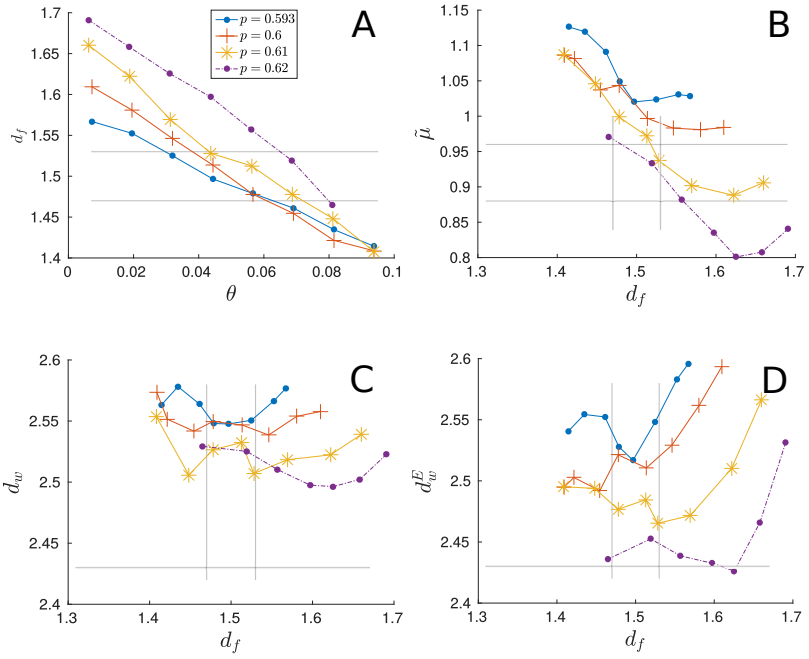

Figure 5.5: (A) Fractal dimension d_f, (B) conductivity exponent $\tilde{\mu}$ (C) walk exponent d_w and (D) walk exponent computed using the Einstein relation d_w^E of θ-subnetworks of percolation clusters generated using threshold probabilities $p = p_c = 0.593$, $p = 0.60$, $p = 0.61$ and $p = 0.62$. Zones delimited by lines represents exponents, with the error intervals, of observed karst networks (Table 5.1). In (C) and (D) only the upper allowed value of d_w is represented by a line.

Dimensionally speaking, a karst network can be a θ-subnetwork of a critical backbone, as the fractal dimension of the backbone is larger than the fractal dimension of observed karst network (Table 5.1). However, at criticality, the conductivity and the walk exponents of θ-subnetworks are, on average, too large (the

curves $p = 0.593$ in Figure 5.5). Thus, we have to consider percolation clusters above the critical probability.

Figure 5.5A shows that the fractal dimension is a decreasing function of θ. For a given θ, the fractal dimension of the generated structures generally increases with the percolation probability p. Meanwhile, the conductivity exponent (Figure 5.5B), for a given d_f, decreases with the percolation probability p. The same remarks hold for the walk exponents (Figure 5.5C). The behaviours of $\tilde{\mu}$ and d_w can be understood intuitively by considering that, as p increases, the number of links of the percolation clusters increases. Thus, on average, the resistance of the percolation cluster decreases and hence $\tilde{\mu}$ decreases. The walk exponent d_w decreases as p increases, since, at a large scale, the percolation clusters are statistically more homogeneous (*i.e.* $d_w \to 2$).

We notice that for $p \geq 0.61$, the θ-subnetworks have a fractal dimension $d_f \approx 1.5$ and also have conductivity exponent close to the one observed for the networks of Tulum (Figure 5.5B). However, the walk exponents of the generated structures are slightly higher compared to the one of Tulum's karst networks (Figure 5.5C).

There is no guarantee that the generated structures respect the Einstein relation. We examine the validity of this relation as a hallmark since this one is satisfied by the karst networks of Tulum and for homogeneous fractal structures such as percolation cluster or the Sierpinski gasket. It is noteworthy that, even if the relation is not fulfilled exactly with the proposed model, the behaviour of the walk exponent computed via the Einstein relation $d_w^E = d_f + \tilde{\mu}$ is similar to the one computed directly by random walk simulation (Figure 5.5D) taking into consideration that the exponents d_f, d_w and $\tilde{\mu}$ are computed using independent measures. As a further step, we study the deviation from the Einstein relation, *i.e.* $d_w - \tilde{\mu} - d_f$ (Figure 5.6). The relation is better satisfied close to p_c and for small θ (*i.e.* large d_f). This is not surprising because critical percolation clusters and their backbones satisfy the Einstein relation up to the scale of the

lattice size.

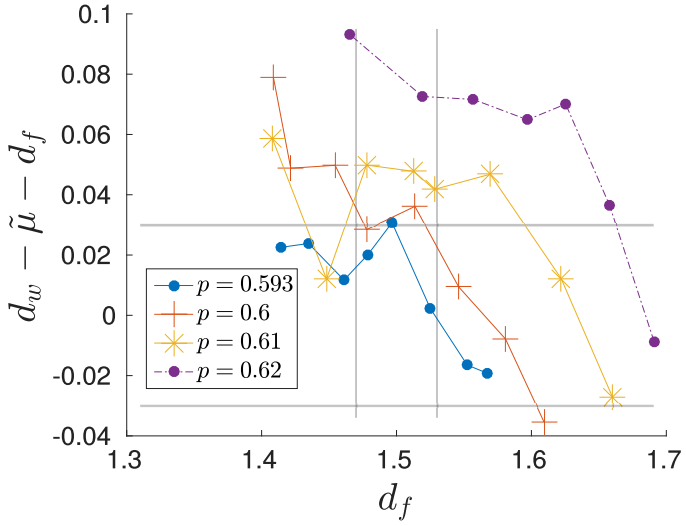

Figure 5.6: Deviation from the Einstein relation. Vertical lines represent Tulum's karst networks fractal dimension, given the confidence interval. Horizontal lines are confience interval given exponents (d_f, d_w and $\tilde{\mu}$) computed on Tulum's karst networks (Table 5.1).

5.3.4 Remark on expected scale behaviours of θ-subnetworks

If we consider θ-subnetworks of percolation clusters above p_c, we lose self-similarity at the large scale. The typical size of percolation clusters is given by the correlation length $\xi \sim |p - p_c|^{-\nu}$. Above and below p_c, clusters are self similar up to the correlation length (ξ correspond to the typical finite size of finite clusters). Above p_c, ξ corresponds also to the size of largest holes on the infinite spanning cluster. If we consider $p > p_c$, ξ is reduced and percolation looks more and more homogeneous (the size of largest holes of infinite spanning cluster are reduced). However, here we consider only θ-subnetworks which

are sparser structures than backbones. The holes (loops) sizes vary non-monotonically with θ. Holes size grows with θ until the θ-subnetwork collapses into a small structure only containing small loops (Figure 5.4). Therefore, the correlation length scale ξ of the substrate (the percolation cluster) is not the correlation length scale ξ_θ of its θ-subnetworks. Nonetheless, ξ and ξ_θ correspond for small θ, *i.e.* close to the backbone. This observation aims to clarify why proper scaling behaviour is expected for θ-subnetwork even above criticality.

5.4 Karst networks and the minimization of dissipated energy and formation cost.

Karst networks are natural systems. Therefore, it is reasonable to assume that they grow in a manner such that the resulting structures minimize the dissipation of energy related to the transport of underground water.

5.4.1 Definition of the energy and calculation

To investigate whether this assumption holds, we compute the (rate of) energy E dissipated by the viscous forces on the θ-subnerworks. Letting R_{ij} be the resistance associated to the link $\langle i, j\rangle$ and Q_{ij} its flow rate, the dissipated energy (assuming a laminar flow described by the Hagen-Poiseuille equation) is given by $E = \sum_{\langle i,j\rangle} R_{ij} Q_{ij}^2$ (see for example Renard and De Marsily [1997]).

The networks generated by our model, whose structures tend to approach the characteristics of real karst networks, are rather different than backbones. However, the backbone of a percolation cluster is the subnetwork that, by maximizing the number of conducting links, minimizes E. Thus, one could expect karst networks to develop until they reach a backbone structure.

Our model is static, meaning we work with a steady state flow and do not allow conduit radii to change over time. Consequently, we cannot study how a karst evolves from its early stage to its maturity. What we can do is to compare the θ-subnetworks with each other to try to understand the structure of observed karst networks.

Our very first hypothesis is that karst systems develop along links carrying the strongest flow rates. One can argue that a strong flow rate is needed to create a link and keep it open. A limiting process of the physics of dissolution is the mass transport. When water dissolves limestone, it saturates in calcite and hence, if there is not a sufficient flux to flush out dissolved calcite, the dissolution process stops. In this way, to guarantee a sufficient water pressure gradient along each links, the network has to concentrate the water flow by limiting the number of conduits. Hence, we are led to consider θ-subnetworks that optimize the dissipated energy for a limited size. Therefore, we make the assumption that karst networks are structures that minimizes

$$C = \sum_{\langle i,j \rangle} R_{ij} Q_{ij}^2 + f(N) \tag{5.1}$$

with $f(N)$ a cost function depending on the number of nodes N of the network. The simplest choice is $f(N) = \alpha N$ with α a constant. We are interested in how C varies with θ. We set the constant to be $\alpha \equiv E_{\max}/N_{\max}$, with $E_{\max} = \max_\theta \{E(\theta)\}$ and $N_{\max} = \max_\theta \{N(\theta)\}$, which has interesting implications. While α looks arbitrary, it is the ratio of two natural constants of percolation clusters. The maximum of N is realized for $\theta \to 0$ by the backbone, whereas the maximum of E is realized by the smallest (in terms of number of nodes N) existing θ-subnetworks which tend to be the shortest path of percolation clusters connecting the two edges of the busbar geometry.

5.4.2 Results

Figure 5.7A illustrates the behaviour of the energy terms for θ-subnetworks extracted from a percolation cluster at $p = 0.60$. When θ increases, the dissipated energy E rises, while the cost of dissolution proportional to N reduces. The overall cost C has a minimum for $\theta \approx 5 \cdot 10^{-2}$. When these results are plotted as a function of d_f (Figure 5.7B), one can see that the dissipated energy E varies abruptly around $d_f \approx 1.52$. The minimum of C is also obtained with this model for $d_f \approx 1.52$.

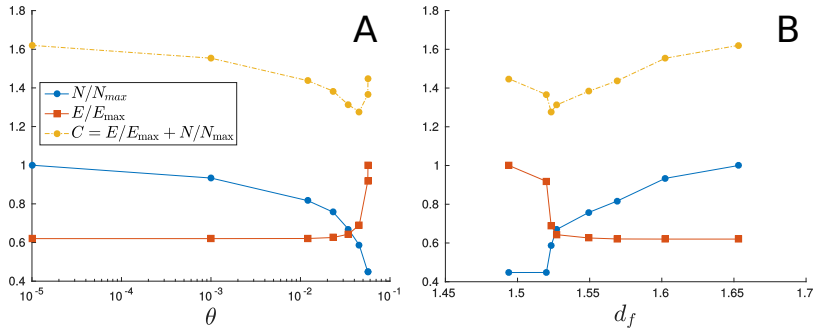

Figure 5.7: Behaviours of the dissipated energy E, the number of nodes N and the function C of θ-sunbetwork extracted from a percolation cluster of percolation probability $p = 0.60$.

To refine the understanding of the links between the structure and the overall energy dissipated in the system, the minimum of C is computed as a function of θ for each set of 6 θ-subnetworks extracted from 400 percolation clusters (100 percolation clusters for each considered p, we work with the same set of θ subnetworks we employ for the Figure 5.5). The average properties of the structures minimizing C are summarized in Table 5.2. The fractal dimensions, conductivity exponents and walk exponents of the structures that minimize C depend on p. The structures exhibiting a similar scaling behaviour than Tulum's karst networks and minimizing C correspond to $p = 0.61$ (excepted the walk exponent, which is too high). For $p > 0.61$,

the properties of the structure of θ-subnetworks deviate significantly from real karst networks.

Table 5.2: Exponents of θ-subnetworks minimizing C.

p	θ	d_f	$\tilde{\mu}$	d_w	$d_w^E = \tilde{\mu} + d_f$
0.593	0.050	1.50 ± 0.04	1.040 ± 0.029	2.56 ± 0.02	2.54 ± 0.05
0.60	0.040	1.53 ± 0.04	0.992 ± 0.030	2.53 ± 0.02	2.52 ± 0.05
0.61	0.038	1.56 ± 0.05	0.919 ± 0.035	2.52 ± 0.02	2.48 ± 0.06
0.62	0.035	1.61 ± 0.05	0.794 ± 0.039	2.49 ± 0.02	2.40 ± 0.07

5.4.3 Discussion about the minimization of C.

Analogy with rivers networks

In Rodríguez-Iturbe and Rinaldo [2001], the authors make a static model of river networks, the Optimal Channel Network (OCN). They assume that a river network develops until it minimizes a functional representing its dissipated energy. The proposed network model minimizes the dissipated energy, and is shown to be statistically similar to real river networks. Since real rivers are not static but rather develop over long time scales, a dynamical model is needed to asses the evolution of river networks. In Banavar et al. [2001], a partial differential equation describing the erosion of an elevation field that represents the landscape is derived. River networks are the drainage directions over the elevation field. It is shown that the stationary solutions of the elevation field equation corresponds to an OCN. The numerical simulations reveal that the model is characterized by a very short time scale, called the freezing time, followed by a much longer time scale, the relaxation time. After the freezing time, the structure of the river network, *i.e.* its drainage directions, does not evolve any more. During the relaxation time, the elevation field is modified but without changing the drainage directions until it reaches a stable configuration characterized by

a drainage network dissipating a minimal amount of energy, an OCN. The fact that the system involves in such a short period followed by a much longer relaxation time that does not change network structure provides an explanation to why river networks of different ages exhibit similar statistical properties. A review concerning these concepts is provided in Rinaldo et al. [2006].

It is temping to assume an analogue dynamical scenario for the description of the development of karst networks: during the short freezing time period, the structure of a karst system quickly takes on the observed structure (described by the minimum of C) and then dissolution widen the conduits over a long period (the relaxation time).

It results from this discussion that the study of the structure of young karst systems, in comparison with mature networks, may support or deny the freezing time hypothesis. However, young karst networks are generally characterized by conduits of small apertures and thus are not directly observable. Therefore, their properties should be studied through dynamical models of dissolution.

Early development of karst networks

Siemers and Dreybrodt [1998] presented a numerical dynamical model of karst network evolution. The dissolution process is studied on networks of fractures that are modeled as percolation clusters above p_c. A busbar configuration is assumed and a prescribed water head difference is imposed between the edges. The percolation networks were built on a 30×30 square lattice. This model shows that the early development stage (that occurs under laminar flow), corresponding to widening of the fractures, determines the structure of the mature karst network. This initial period is brief compared to the entire evolution of the network toward its maturity. The authors show that preferentially dissolved fractures correspond to those forming the pathways offering the least resistance to the flow. However, for percolation probabilities $p > 0.67$, calcite undersaturation mechanisms

also play an important role in the selection of preferentially dissolved fractures[3]. For percolation probability close to p_c, there is a small number of pathways offering small resistances to the flow, and these pathways are decisive for the resulting karst network structure and the details of the undersaturation process is not important.

The model of Siemers and Dreybrodt [1998] was designed to study the development of predominantly vertical karst networks. The dissolution process acts from the upper edge to the bottom edge, with the results that the water saturates in calcite while it enters in the network. However, the networks of Tulum are extended horizontal structures on which it is expected that rainfall water contributes to the injection of non saturated (in calcite) water over the catchment areas. In addition, the dissolution process of Tulum's karst networks is also highly determined by the sea water intrusion. Therefore, the analogies with this model has some limitations.

To conclude, in the work of Siemers and Dreybrodt [1998], we recover the notion of the freezing time which is a short period at the early development of the networks during which the final structure of the karst networks is determined. Moreover, for percolation probability $p \lesssim 0.67$, they show that the pathways of least resistance (which corresponds in our model to the θ-subnetworks) determines the network structure. This is an additional argument that indicates that our proposed model and global minimization principle are reasonable.

[3]In Siemers and Dreybrodt [1998] a bond percolation model is used to generate the fracture networks. For bond percolation on a square lattice, the critical probability is $p_c^b = 0.5$, with p^b the bond percolation probability. The authors show that the details about the dissolution of calcite is determining for final network structure when $p^b > 0.6$ which correspond to $p \gtrsim 0.67$ for site percolation.

5.5 Conclusion

The model presented here aimed to reproduce the observed exponents (fractal dimension, conductivity exponent and walk exponent) of karst networks of the area of Tulum. We studied the dissipated energy due to viscosity E and the cost (proportional to the number of nodes N) associated to the formation of the structures (θ-subnework) generated by the model.

We showed that for ranges of site occupation probability close to p_c, the generated structures minimizing $C = E + \alpha N$ exhibit similar scaling behaviour to the Tulum karst networks. The precise value of the constant α determines the minimum of C. Using physical arguments, we introduced a cost function that prevents the system from becoming too extended with the aim to keep the dissolution process active. However, however more work is needed to better define the functional C.

A study of statistical properties of the structure of younger karst networks, and the set up of a dynamical model of dissolution adapted to Tulum's karst networks, could provide interesting additional information to assess the freezing time hypothesis, and may ultimately reinforce our approach.

Although our model reproduced the fractal dimension and conductivity exponent of karst networks quite well, it failed to reproduce the walk exponent accurately. Improvement of the measure of d_w, using for example the probability of first-passage time of random walk, should be considered. The results may confirm or deny the violation of the Einstein relation by the generated structures.

Others percolation models such as directed percolation Hinrichsen [2000] and percolation with long-range correlation Prakash et al. [1992] provide interesting features for karst modelling. A cluster generated by directed percolation exhibits a spatial anisotropy such as the one observed looking at the main conduits orientation of Tulum's karst networks (see Figure 5.2). Percolation with long-range correlations generate spatially correlated clusters in a similar way as dissolution creates correlated voids

in rocks. However, fractal properties of the generated structures of both percolation models differ from those of the networks we want to model.

The multifractal properties of moments of flow rate (current) distribution is an important research topic for characterizing random resistor networks Redner [2012], Stenull and Janssen [2001]. Here we studied flow rate distributions truncated by the parameter θ. A more detailed study of their properties could help improve the understanding of the properties of the θ-subnetworks and constitute a possible direction for future research.

Finally, our model relies on the fine tuning of the percolation probability p and on the flow rate threshold θ. However, a karst network is a natural system and it is expected that it develops naturally towards the observed self-similar structure in a generic way (*i.e.* as a system having a critical point as an attractor of its dynamics without needing to tune any parameter in a precise manner). Generic scaling behaviours are features of self-organized criticality Pruessner [2012] or the Kardar-Parisi-Zhang equation Kardar et al. [1986] (among others). In our model, the minimum of the function C characterizes the attractor because karst networks are expected to be structures that minimize C. Thus, to avoid fine tuning, a dynamic stochastic equation for karst networks that evolves, in a generic way, to the minimum of C should be considered.

Chapter 6

An application of the karst network model

6.1 Introduction

The area of Tulum, including the nearby coral reef and the Sian Ka'an Biosphere, is highly vulnerable to water pollution due to the development of the tourism industry.

In this Chapter, we use the previously developed model (Chapter 5) to generate realistic karst networks in areas, located in the vicinity of the town of Tulum, where we expect to find conduits but which are still not fully explored by the cave divers. The study area hosts Ox Bel Ha, a part of Sac Actun and some other smaller networks. It is supposed that, due to the similarity of the geology and as suggested by the geophysical airborne investigations of Schiller et al. [2015], these networks are connected. Therefore, we aim to connect the simulated networks with the real networks to obtain an overall connected structure covering the study zone. This is a prerequisite to simulate groundwater flow and contaminant transport in the area.

The main water pollution source is the town of Tulum since only a small part of the urban wastewater is treated. However, this area is poorly explored by cave divers (due to pollution) and we lack the maps of the expected conduits that connect the

town to the sea. In addition, the results of airborne survey above Tulum are not exploitable because Tulum's electromagnetic pollution. Other areas are less explored as a result of accessibility issues of sinkholes (no road, deep forest, ...), or even because of the lack of sinkholes. In the north of the domain, two waste dumps are additional sources of contamination.

We previously characterized Tulum's networks by their fractal dimensions, walk exponents and conductivity exponents (Chapter 3 and 4). These three exponents are intensive properties *i.e.* they do not depend on the system size (the number of nodes). We take advantage of this observation in this application to extend the real networks keeping invariant their properties.

The overall generated structure together with field data are used to model the water flow over the area as a preliminary step to assess its pollution vulnerability.

In Section 6.2, the methodology employed for generating the networks is presented. Next, in Section 6.3, we study the properties of the overall generated connected network. In Section 6.4, we present the flow model of the area of Tulum.

6.2 Methodology

The study zone is partially covered by known karst networks. Some parts remain unexplored or are currently under exploration. These parts are delimited by polygons in Figure 6.1A. Contact points between polygons and known networks (small squares in Figure 6.1) are employed as given inlets and outlets to generate the networks.

We fill these polygons with percolation networks (Figure 6.1B). More precisely, we generate percolation clusters, in a polygon, until a realization is such that the largest cluster (the infinite spanning cluster) connects all the contact points. The percolation cluster is built from a square lattice filling the polygon. We use the percolation probability $p = 0.61$ to maximize the probability to generate networks exhibiting the expected

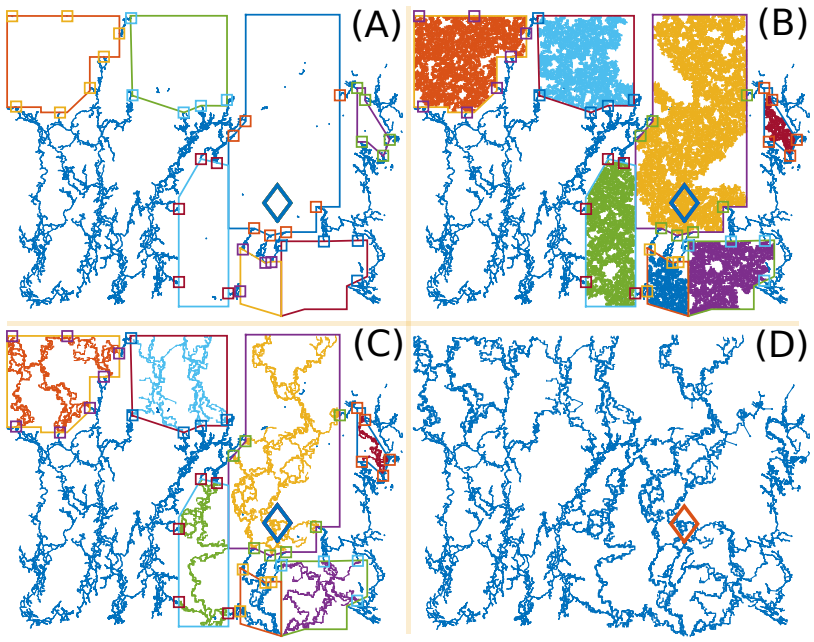

Figure 6.1: Example of a simulation of a network filling the area of Tulum (the location of the town is indicated by the thick diamond). Polygons are the areas where we generate networks (A). Small squares are points of already explored network that intersect polygons. (B) Percolation clusters generated with $p = 0.61$. (C) θ-subnetworks of exponents $d_f \approx 1.5$, $\tilde{\mu} \approx 0.9$ and $d_w \approx 2.4$. (D) Resulting network.

scaling behaviours (Chapter 5).

From the infinite spanning clusters (in the following we mention them, simply, as percolation clusters) we extract subnetworks. We solve the Kirchhoff equations for laminar flow on each percolation clusters, considered separately from the remaining of the structure. We impose the contact points as inlets and outlets. Moreover, nodes of percolation clusters located on edges of polygons and corresponding to the upper border of the studied area are also taken as inlets (we defined in the same way outlets which are nodes of edges located on the lower part of the domain

(the sea)). Given these boundaries, we obtain the backbone (the conducting part) of the percolations cluster of each polygon.

At this point, we extract from each backbone the θ-subnetworks of fractal dimension in the range $d_f = 1.5 \pm 0.03$ (Figure 6.1C). Practically, on a given backbone, we extract a set of θ-subnetworks corresponding to different values of θ and chose the closest one to $d_f = 1.5$. We showed in the Chapter 5 that for $p = 0.61$ the conductivity exponents $\tilde{\mu}$ of θ-subnetworks of dimension $d_f \approx 1.5$ are expected to be around $\tilde{\mu} = 0.92$, if not, a new percolation cluster has to be generated. The same remark holds for the walk exponent. However, we are more flexible with the value of d_w, since we already know (see Chapter 5) that our model has some difficulties to reproduce this exponent. Note that, after the simulation we compute the properties of the connected final structure. The large extension of the resulting network attenuates finite size effects and impact less the computation of d_w.

The simulated structure, *i.e.* the connected network spanning the domain (Figure 6.1D), contains a large number of nodes $N \approx 4 \cdot 10^4$. A by-product of the computation of the fractal exponent is the coarse graining of the structure which can be useful for flow simulation (Figure 6.2). As an indication, the size of a standard mesh needed to cover the non renormalized network is around $2 \cdot 10^5$ elements. Note that we generate the percolation cluster on a regular grid. Another effect of the coarse graining is to smooth nodes positions.

6.3 Properties of the overall connected network

The aim of this application is to extend already explored networks in a way that the overall structure is similar to observed parts. We compute, as an *a posteriori* validation of the procedure, the exponents of the simulated structure.

To stay computationally efficient, we chose to generate the

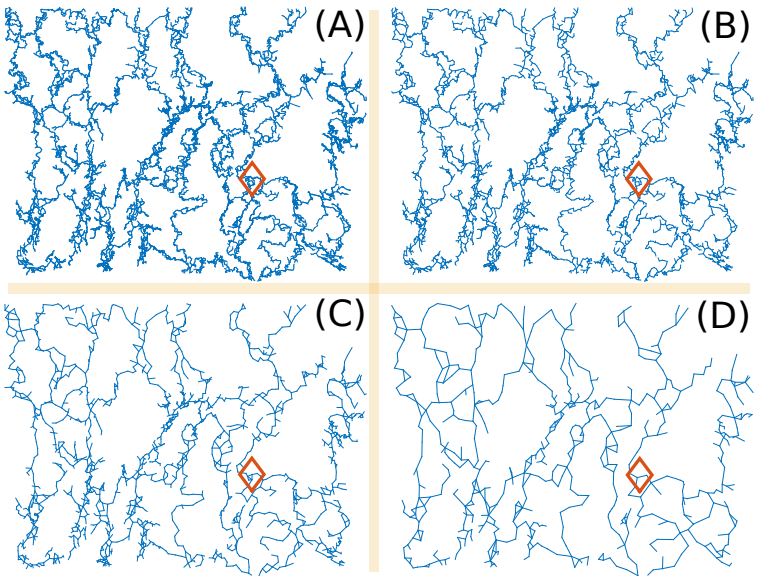

Figure 6.2: Coarse graining of a generated network using the Maximun-Excluded-Mass-Burning algorithm Song et al. [2007]. From step 1 (A) to step 4 (D). Here, box size is $l_b = 2$.

percolation cluster on a square grid of size $\lambda' = 4\lambda$ with λ the mean size of links of the mapped networks. This grid parameter corresponds to a grid made of $6{\cdot}10^4$ nodes for the largest polygon (the one in which Tulum is enclosed Figure 6.1). If we want to increase the grid precision by a factor 2 it corresponds to multiply the number of nodes by ≈ 4 which begins to be very CPU demanding for the calculation of the percolation backbone.

Thus, the generated structure is made of two grids of different grid parameters. This issue implies careful considerations on the way we compute network's exponents.

The computation of the fractal dimension, using the method described in Chapter 3 Section 3.2, relies on the hypothesis that the distribution of link sizes is peaked around its mean value. The link sizes distribution is smoothed with the coarse graining (Figure 6.2 and 6.3). Indeed, the nodes of the coarse grained structure are located at the barycentre of boxes from which they

are built (see Chapter 3), which averages out grids precision difference (as long as the difference between λ and λ' is not too large). Therefore, we do not notice a major influence on the computation of the fractal dimension since the confidence interval is rather small (Figure 6.4).

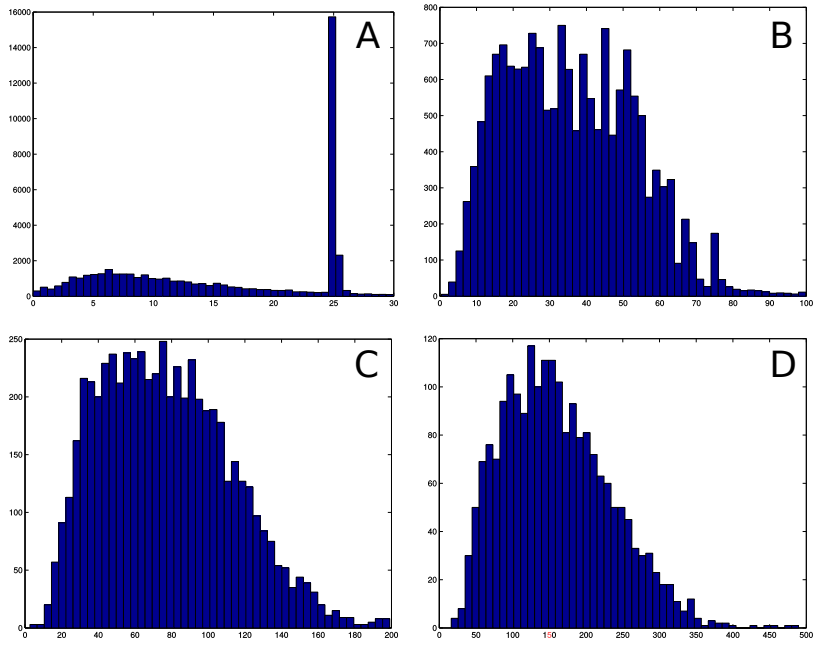

Figure 6.3: Distribution of links size in meter. (A) Simulated network, the peak around 25 m corresponds to the percolation cluster grid size, the peak around 6 m corresponds to mean link size of real mapped networks. (B), (C) and (D) link size distribution after first, second and third renormalization steps. Links size distribution is smoothed by the coarse graining procedure. The employed box size is $l_b = 2$.

We observed that the computation of the conductivity exponent is not very sensitive to the difference between grids, the reason is the following. The resistance between two linked nodes is proportional to the distance separating them (Hagen-Poiseuille), which in average compensate grids disparities. This dependence

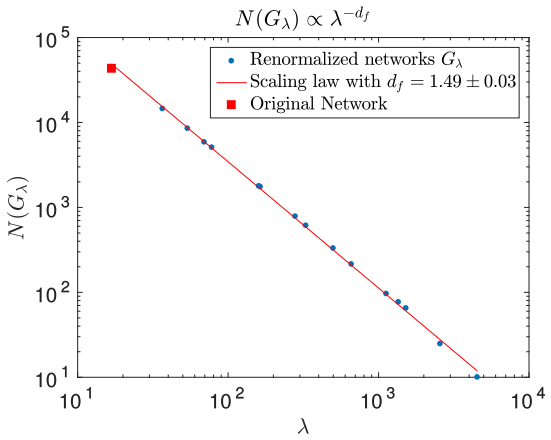

Figure 6.4: Fractal dimension of simulated network.

of the resistance according to link size explains why, when we renormalize the networks, the computed conductivity exponent is reasonably invariant (Figure 6.5B).

The computation of the walk exponent on the overall structure is more delicate. Due to the large sizes of the generated and the real networks some walks may occur only on the simulated part or, only on the real networks part. Imagine two walkers, one stepping on a structure of mean links size λ and the other one walking on a structure of mean links size $\lambda' > \lambda$. We stop the two walks when each one reaches a mean square displacement of L. As a result of the links size difference, the walk duration (in average) is t for the first walker and $t' < t$ for the second. Here, the considered structure exhibits two different grid sizes. We have to take this effect into account for the computation of the walk exponent. Thus, we put a weight on the walk duration time for the computation of the mean square displacement:

$$\langle r^2(t)\rangle^W = \frac{1}{t^W}\sum_{i=1}^{t} \|r(i) - \bar{r}\|^2 \tag{6.1}$$

with $\bar{r}$ is the time average of the position r of the walker and

t^W is defined as

$$t^W = \sum_{i=1}^{t} \|r(i) - r(i-1)\| \tag{6.2}$$

with $\|\cdot\|$ the Euclidean distance. The resulting walk exponent is noted d_w^W. Thus, if the walk occurs only on the real networks (respectively only on the simulated part) the weight is $t^W = t\lambda$ (respectively $t^W = t\lambda'$). In such cases $\langle r^2(t)\rangle^W \propto \langle r^2(t)\rangle$, and hence $d_w = d_w^W$. However, if the walker steps on both parts, t^W is averaged between $t\lambda$ and $t\lambda'$ and $d_w \neq d_w^W$.

Table 6.1: Exponents of Ox Bel Ha and simulated network of Figure 6.1.

	Ox Bel Ha	Simulation
d_f	1.51 ± 0.03	1.49 ± 0.03
d_w	2.39 ± 0.03	2.49 ± 0.03
d_w^W	2.40 ± 0.03	2.42 ± 0.03
$\tilde{\mu}$	0.92 ± 0.04	0.93 ± 0.01

Another way to palliate the grid size differences is to compute the (non-weighted) walk exponent directly on renormalized network, as the procedure smooth the difference $\lambda - \lambda'$. Results are presented in Figure 6.5. The effect of the coarse graining, at the first step, is to lower the walk exponent value, from 2.49 to 2.46. We also compute the corresponding values of d_w^W. Links length differences are attenuated as we renormalize the network, therefore the weighted walk exponent is closer to the non-weighted far from the original network. For completeness the value of $\tilde{\mu}$ along renormalization is given (Figure 6.5B). Notice that computed exponents are quite robust to renormalization close to the original network.

Under these considerations, the generated structure extends already mapped networks and exhibits fractal properties close to real karst networks hosted in the area. Resulting overall networks properties are listed in Table 6.1.

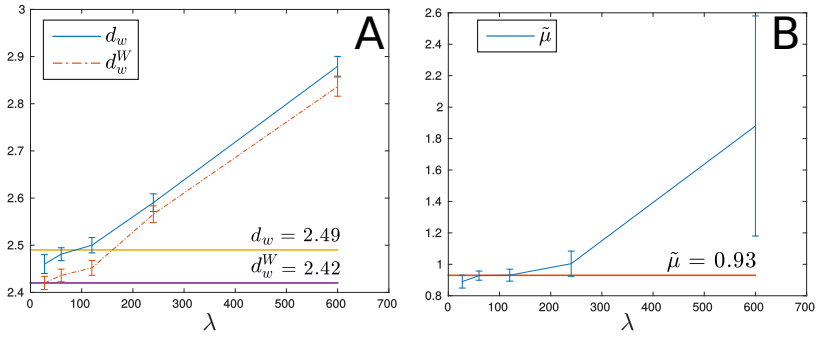

Figure 6.5: (A) Walk exponent d_w, weighted walk exponent d_w^W and (B) conductivity exponent $\tilde{\mu}$ along renormalization. Lines represent exponents computed on the non renormalized simulated network (Table 6.1). λ is the mean links size at each renormalization steps. In (A) and (B) plotted values for $\lambda < 300$ correspond to the renormalized networks (A), (B), (C) and (D) of the Figure 6.2

.

6.4 Groundwater flow model of the region of Tulum.

6.4.1 Introduction

To characterize the groundwater dynamics in the area, we have installed a piezometric network, recording the water level during 2 years with a time steps of 15 minutes (from 2013 to 2015), on a 10 km transect linking the shore to the upper parts of Ox Bel Ha which are Kaan Luum and Lago Union (Figure 6.6). The sea tides are propagated inland and measured by the probes. When propagating toward inland, the sea signal is damped and phase shifted. The comparison between the input signal (the sea water level) with the measured one in different places along the network allows gaining information about the network's structure.

In addition, in 2016, a master student, Grégory Kaeser sampled water and studied the water quality in this region (Fig-

Figure 6.6: Map of the piezometric network. (Yellow) points indicate the emplacement of water level sensors.

ure 6.7). The aim of his work was to assess the extend of a pollution coming from Tulum and from the upstream part of the Ox Bel Ha system where a new garbage discharge is located (Figure 2.2). These two important sources of pollutions are not connected to the main explored networks via known conduits but the map of contamination obtained by G. Kaeser suggests clearly that there was contaminant migration (Figure 6.8). Therefore, we generated networks to fill exploration gaps and obtained an overall connected structure on the study area. It may be possible that this assumption leads to an overestimation of the real conduits density. However, this assumption allows us to consider the worst conceivable scenario in terms of networks' connectivity.

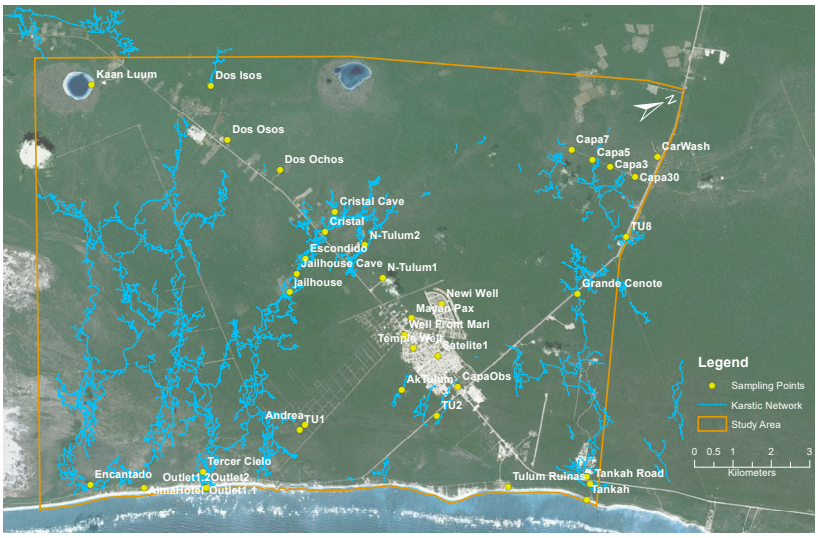

Figure 6.7: Map of the location where water was samlpled.

6.4.2 Flow model

To study groundwater circulation on the generated structure, the groundwater software modelling FeFlow was used by G. Kaeser under our supervision. More precisely, for computational efficiency, the model is based on the coarse graining of the realization presented in Figure 6.2C. We shown, in Figure 6.5, that this renormalized network still exhibits the realistic karst network properties.

To account for non linear head losses in conduits, the water flow is simulated using the empirical Manning–Strickler formula [Manning et al. [1890]]

$$V = K_s R_h^{2/3} S^{1/2} \tag{6.3}$$

with V the average velocity on the conduit cross-section, K_s the friction coefficient, R_h the hydraulic radius (here we consider flooded conduits thus $R_h = r/2$, with r the conduit radius), S the hydraulic head loss.

We impose, as a boundary condition along the shore, a real-

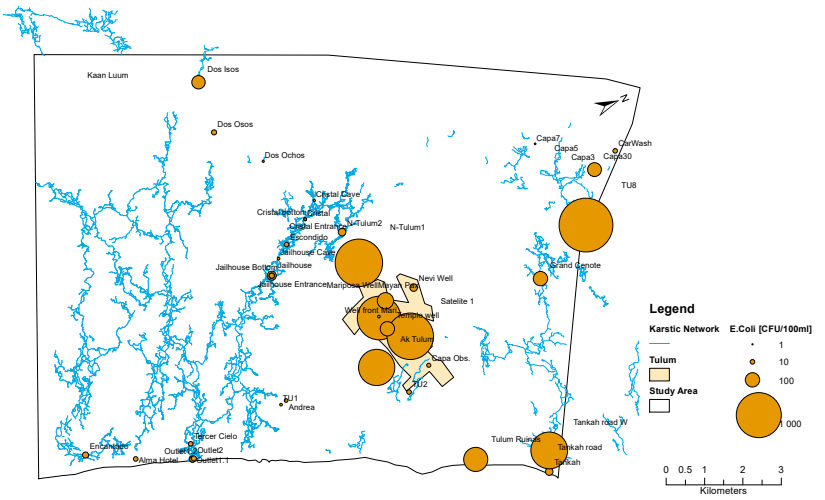

Figure 6.8: Concentration of Escherichia coli over the study area.

istic sea tide signal (based on the data of a probe monitoring sea water level of the area). We aim to reproduce with the model, at the probes locations, the observed sea tide damping and phase drift. For this the parameters of the Manning–Strickler formula are tuned to obtain the expected behaviours. Doing that we obtain conduit radii around 3 m. It results in a regional water level gradient about 10 cm/km (which coincide with the field observations made by us as well as [Bauer-Gottwein et al. [2011]]). The friction coefficient is set (arbitrarily) to a typical value of $K_s \approx 200\ s/m^{1/3}$. The obtained water level field is presented in Figure 6.9. The details of the calibration and the sensitivity analysis are discussed in the MSc thesis of G. Kaeser [Kaeser [2016]].

Next, based on this calibration, pollution scenarii can be studied. As a preliminary result, we compute the time needed for a particle to flow between the town of Tulum and the shore (it corresponds to a land distance around 5 km). We attained travel time ranging from 5 to 15 days, depending on the exact location where particles are released and on the tide cycles. These results

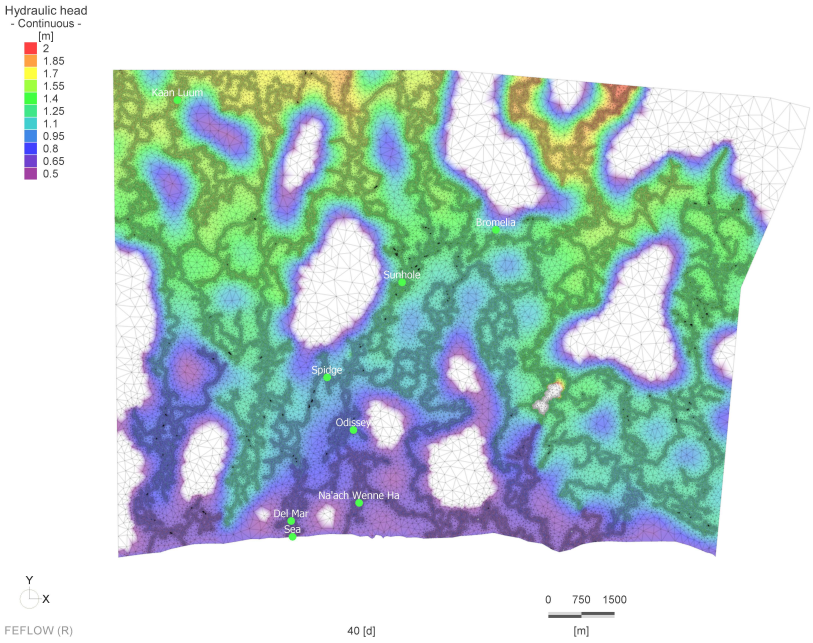

Figure 6.9: Water level obtained calibrating the model.

match with previous tracer tests we carried out in 2013 and 2014 in the karst conduits of Ox Bel Ha, we measured travel times about 1 km/day (which are also close to the results reported in Beddows [2004]).

The networks geometry and properties depend on the realizations. To asses this variability we study others simulated networks (Figure 6.10). We also work with the third renormalization steps (using a box size of $l_b = 2$) of each realization.

We keep the same Manning–Strickler parameters as those previously obtained from the sea signal calibration on the first studied realization and investigate the sensivity of the solution to the detailed geometry of the networks. We find that at this scale, the results are rather robust since, on this set of realizations, the expected damping and phase drift at our control points (Figure 6.11) are reasonably well reproduced. We also find a travel time between Tulum and the shore ranging from 5

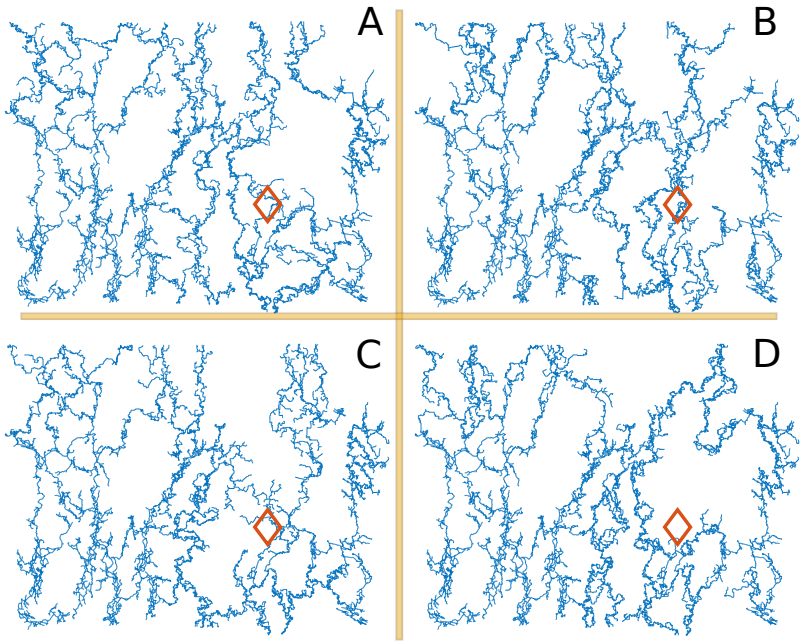

Figure 6.10: 4 realizations built with from the same set of polygons presented in Figure 6.1.

to 15 days.

These results are preliminary, extended simulations are needed to produce reliable information about contaminant transport. The study of the variability of hydraulic properties has to be assessed on a larger set of realizations, however we notice that the results are comparable even if the conduits locations varies from one realization to another.

6.5 Discussion and Conclusion

It is important to notice that the aim of this work is not to predict the real location of the karstic conduits. We built this model in such a way that simulated networks are similar to real karst networks. It is analogue to the strategy adopted in statistical

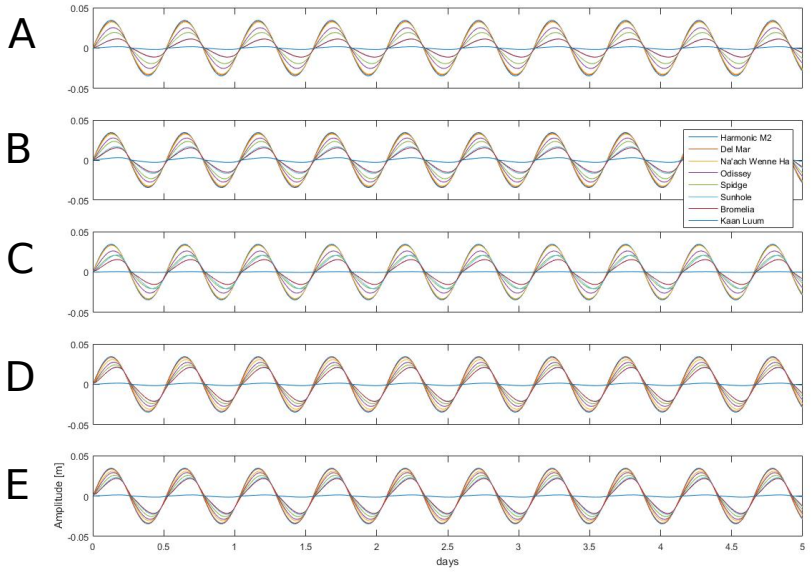

Figure 6.11: Sea tides signal mesured on our models at probes' locations. (A) is the calibrated realization. The RMSE, between the real measured amplitudes and simulated amplitudes is about $2 \cdot 10^{-3}$ m. (B), (C), (D), (E) mesured signals on for the realizations presented in Figure 6.10. The RMSE is between 3 and $7 \cdot 10^{-3}$ m. Notice that we imposed the same Manning-Strikler parameters (the calibration) on all realizations.

physics. For example, the knowledge of the exact position of the particles of a gas is not necessary to study macroscopic observables such as temperature or pressure (see Chapter 1). Over a large set of realizations the distribution of conduits location is homogeneous except near the imposed contacts points (Figure 6.12), hence the model explores the space of possible networks exhibiting similar properties than Tulum's network quite well.

A great number of different realizations can be generated (the computation time of a θ-subnetworks in the largest polygon is about 10 minutes, examples of other realizations are pre-

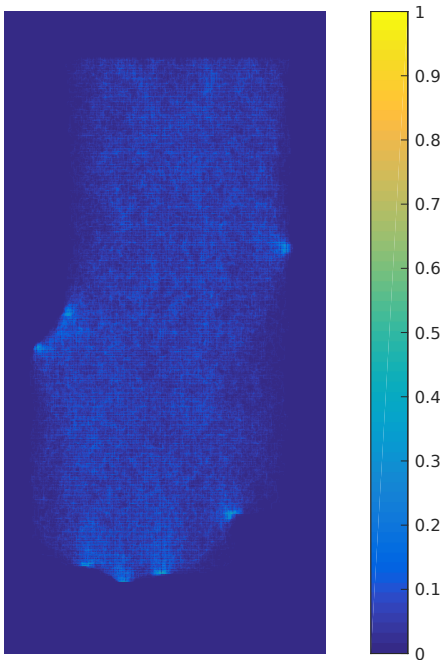

Figure 6.12: Probability presence of a conduit (a pixel represent a 30×30 m^2 square) generated from 100 simulated networks in the polygon containing the town of Tulum (Figure 6.1)

sented in Figure 6.10). A careful study of how the flow properties of these networks (such, *e.g.* the arrival time of a pollutant) depends on a realization has still to be done. The variability between the realizations of such kind of network's macroscopic properties (*i.e.* on larger length scale than link sizes) has still to be assessed. Since generated structures are built to be statistically the same fractal object it is expected their macroscopic properties are peaked around their means. Early results presented in Section 6.4 are encouraging.

This chapter shows the ability of our simple karst model to be applied to a real-world problem. An extension of the model to 3 dimensions would be interesting to enlarge the applicability of the model. However, this requires first to proceed with a complete 3 dimensional characterization of real karst networks

to allow assessing the relevance of the model in more general geometry.

Chapter 7

Conclusions

Our work aimed to find common characteristics of karst systems. For this, we studied the karst networks of Tulum. Since they are embedded in the same environment, it is easier to point out their similarities. The karst systems of this area are particular because they form very long networks. Moreover, due to the weak tectonic activity of the Yucatan peninsula, there is no large scale (*i.e.* at scales of the order of the size of the networks) geological bodies (faults, fractures) that constrain their development. The heterogeneities (fractures, rocks properties) are observed at the meter scale. The growth of the networks is driven by the regional hydraulic gradient which is small, around 10 cm/km due to the low topography of the region. Therefore the structure of the networks is shaped by the small scale heterogeneities and, at large scale, by the spatial anisotropy created by the overall regional hydraulic gradient which induces a preferential flow path direction perpendicular to the sea shore.

7.1 Main results

In Chapter 1, we fixed the main objectives of the thesis in the form of questions. In this section, we summarize what we learned through our work.

Do karst networks exhibit scale invariant properties?

Previous research conducted in a broad variety of fields has shown that scale invariances are common features of natural systems. In this thesis we studied scale behaviours of karst networks in the region of Tulum (Chapter 3 and 4). We focused on maps of explored karst networks which are spatially embedded networks (*i.e.* graphs whose nodes are located on a physical space). We compute their fractal dimensions using a real space renormalization scheme developed by Song, Havlin and Makse [2005]. Next, we analysed their associated conductivity properties. For this, we solved the Kirchhoff equations assuming an Hagen-Poiseuille flow on each link of the graphs. And finally, we considered diffusion properties by simulating random walks and computing their mean square displacement.

It results from these measurements that the karst networks of the area of Tulum are characterized by a similar fractal structure. The conductivity between two network's nodes follows a power law depending on the Euclidean distance separating them (the exponent of the power law is named the conductivity exponent). The root mean square of the walker's displacement is a power law the walk duration. The observed diffusion is anomalous and subdiffusive and is characterized by the walk exponent. The networks studied are characterized by similar sets of fractal dimension, conductivity and walk exponents. These exponents are not independent and are approximately related through the Einstein relation.

Are we able to build a model of karst networks reproducing the observed scaling properties?

Chapter 5 aimed to understand the structure of the karst networks of Tulum. For this, we built a model capable of generating networks showing structure similar to the observed one. The karst systems around Tulum transport water through networks connecting the inland to the sea (the flow of water is driven by the regional hydraulic gradient). The model is based on per-

colation theory which is the archetype model for the study of connectivity properties of a system. To allow water transport, a cluster connecting the inlets and the outlets is needed. Therefore, we studied the percolation model close to criticality where there is a cluster that spans the domain. Such clusters are self-similar, their walk and connectivity exponents are well studied. The conducting part, *i.e.* the links carrying non zero flow rate, of a percolation cluster is the backbone and also exhibits anomalous diffusion and a power law conductivity. We examined the θ-subnetworks of percolation backbones. A θ-subnetwork is the part of the backbone connecting the boundaries of the domain whose links carry a flow rate above a given flow rate threshold θ. By tuning θ, we were able to generate networks that exhibit similar fractal and conductivity exponents to those characterizing the karst networks of Tulum. However, we met difficulties to reproduce exactly the observed walk exponent. We do not clearly understand why, therefore further investigations are needed.

Can we understand, based on the model, the overall structure of karst networks?

The backbone of a percolation cluster is the structure that transport water for a minimum of dissipated energy caused by friction forces since it maximizes the number of links. The dissipated energy of θ-subnetworks grows with θ, while the number of nodes of the structure decreases as θ increases. Therefore they dissipate more energy than the backbones.

Let's imagine that a percolation cluster is the network on which a karst grows. It is natural to assume that the karst system develops while optimizing the transport of water in terms of dissipated energy. Therefore, it dissolves rocks to create conduits (links) and hence develops until it reaches a backbone structure. Our model is static. Its aim is to reproduce the structure of karst networks as observed now. Thus, we cannot study the dynamic of their development but we study ensemble of θ-subnetworks to learn about their structures.

We numerically showed that θ-subnetworks having a similar structure than Tulum's networks minimize the sum of the dissipated energy and a function proportional to the number of nodes (the size of the network). Thus, based on this model, we made the hypothesis that karst networks are structures that develops to optimize the transport of water for a limited size. To keep the dissolution process active, the saturated in calcite water has to be flush out. Therefore, a sufficient flow rate on each links is necessary. Thus, the water is constrained to flow on a subnetwork of the backbone which has an energetic cost that we named the formation cost.

Since karst networks develop over extremely long periods, one could wonder how and why the systems relax to the currently observed structure. Dynamical models of the development of river networks show that the systems structure is imprinted with a very short period (named the freezing time) at the beginning of its growth, [see the review Rinaldo et al. [2006]]. This explains why young and mature river networks exhibit the same statistical properties. An analogue phenomena is observed in models of the early development of karsts. This early stage, characterized by laminar flow, occurs over short period (which is the analogue of the river's freezing time) and is determining for the final networks structure [Siemers and Dreybrodt [1998]]. However more work are needed to validate or not our assumptions, for example a detailed study of the influence of the turbulent flow phase on the final structure of extended networks. Some work has been done in this topic [Howard and Groves [1995]], but the limited size of the studied structures and the particular geometry of used for the fracture networks (a regular homogeneous lattice) makes the results hard to be transposed to our work.

Other results

In Chapter 6, we used the proposed model implemented to generate karst networks in unexplored areas around Tulum. The

aim was to set up a regional groundwater flow model based on real data coming from water level probes installed in the field. This model is a preliminary step that may help assess the vulnerability of the environment to water pollution. Early results are encouraging with respect to our methodology. The study area included the mapped karst networks and we connect them through stochastically generated networks allowing to obtain an overall connected network exhibiting realistic karst properties. Flow simulation was used to calibrate the model (like the conduits radii since our model do not provide this information) to fit with the probes' data. Early results, such as the computation of the travel time for a particle to flow from the town of Tulum to the sea, are encouraging since they reproduce expected values. A regional water flow model of the area is crucial for the management and the protection of the underground water because of the development of tourism.

7.2 Discussion and future developments

The fractal dimension is not sufficient to fully characterized a fractal structure. More scaling laws are needed to better describe it, however it is not known exactly how many. We chose to focus on the fractal dimension, conductivity and walk exponents because they are the most standard ones listed and they are related by the Einstein relation. However more properties about networks should deserve attention such as the distribution of the hole sizes (unkarstified area delimited by conduits) or the length of the path linking two nodes compared to the Euclidean distance separating them (named tortuosity by geomorphologists). Moreover, these measures can also be computed on θ-subnetworks to better assess the similarities, or the lack of similarities between real networks and generated ones.

Cavers map karst networks all over the world. A systematic analysis of their properties would be interesting. However, the

geological environments in which karsts are embedded have to be considered carefully since it may constrain strongly the observed structures. Generally, karst networks can not be considered as systems embedded in two dimensions. Hence, if they are fractal structures, they may be characterized by fractal dimensions between 2 and 3.

Depending on what we learn by analysing true 3-dimensional karst networks, it would be interesting to extend the model proposed in this thesis by considering percolation backbones in 3 dimensions. It is possible to introduce main geological constraints imposing quenched disorder (*i.e.* disorder that do not depend on time, "frozen" disorder) in the model. Here, it means to fix lattice sites to be empty or occupied according on whether we want to avoid or impose conduits somewhere. However, these additional constraints may strongly affect the model near the critical point, or even avoid phase transition (since for example a cluster of quenched empty sites may prevent spanning clusters). In fact, imposed contact points in the application described in Chapter 6 can be understood as quenched disorders. However, we did not impose them directly as occupied sites, as we rather sampled preferentially by spanning percolation clusters connecting these points. This procedure was possible since this conditioning was not too strong.

The comparison of the structures of young and mature karst networks have to be examined to study the relevance of the freezing time hypothesis. However, it may be a hard task due to the diversity the geological environments encountered. In addition, young karst networks are characterized by small conduits which are not directly explorable. Thus, young karst networks may be studied through numerical model.

An important research topic related to our work is the study of directed path in random media [Kardar and Zhang [1987]]. A directed path between two points is a path presenting no loops and no overhangs. It can be thought as the trajectory of a particle driven by a field (the dynamical interpretation). Each directed path may be associated with a weight that represents

its occurrence probability. It is observed that in random media (such as the random bond Ising model) optimal paths (path of largest weights) go through impurities (they are said to be pinned to impurities) and form complex loopy structures. For a pedagogical introduction see [Kardar [2007]].

Water flowing in karst networks follows directed paths. In our model flow rates carried by each link may be considered as a weight. Thus, with this definition it is possible to study the probability of observing a given path. Impurities may be viewed as red bonds. The backbone between two percolation network's nodes is characterized by particular links (the red bones) which concentrate all the flow rate in such a way that the severing of a red bone stops the flow between the two nodes. Thus flow paths are pinned to red bones. Thus our model is close to a well studied and mathematically developed branch of physics which may motivate some further theoretical developments.

On a wider perspective, it may be interesting to try to sort karst networks into a universality class. It has to be done through a model of karst. For example, using our model, the properties such as the order parameter and the θ-subnetworks correlation length ξ_θ, have to be studied close to the critical point for relevant θ. As noticed, in Chapter 5, the correlation length ξ_θ is different to the one of percolation cluster since they are sparser objects than the backbone. Therefore, a careful study of the θ-networks property in function of the distance to criticality $|p - p_c|$ has to be done (p_c is the critical probability of the percolation model).

Other models of karst networks should also be assessed to avoid, for example, the fine tuning of parameters or the laminar flow hypothesis. The study of a system using diversified approaches is often useful to try to reach its essence.

Bibliography

Per Bak, Chao Tang, and Kurt Wiesenfeld. Self-organized criticality: An explanation of the 1/f noise. *Physical Review Letters*, 59(4):381, 1987.

Per Bak, Kan Chen, and Chao Tang. A forest-fire model and some thoughts on turbulence. *Physics Letters A*, 147(5):297–300, 1990.

Jayanth R Banavar, Francesca Colaiori, Alessandro Flammini, Amos Maritan, and Andrea Rinaldo. Scaling, optimality, and landscape evolution. *Journal of Statistical Physics*, 104(1-2): 1–48, 2001.

Albert-László Barabási and Réka Albert. Emergence of scaling in random networks. *Science*, 286(5439):509–512, 1999.

Marc Barthélemy. Spatial networks. *Physics Reports*, 499(1): 1–101, 2011.

Peter Bauer-Gottwein, Bibi RN Gondwe, Guillaume Charvet, Luis E Marín, Mario Rebolledo-Vieyra, and Gonzalo Merediz-Alonso. Review: The Yucatán Peninsula karst aquifer, mexico. *Hydrogeology Journal*, 19(3):507–524, 2011.

Patricia Anne Beddows. *Groundwater hydrology of a coastal conduit carbonate aquifer: Caribbean coast of the Yucatan Peninsula, Mexico.* PhD thesis, University of Bristol, 2004.

Daniel Ben-Avraham and Shlomo Havlin. *Diffusion and reactions in fractals and disordered systems*. Cambridge University Press, 2000.

Andrea Borghi, Philippe Renard, and Sandra Jenni. A pseudo-genetic stochastic model to generate karstic networks. *Journal of Hydrology*, 414-415(1):516–529, 2012.

Dante R Chialvo. Critical brain networks. *Physica A: Statistical Mechanics and its Applications*, 340(4):756–765, 2004.

P. Collon-Drouaillet, V. Henrion, and J. Pellerin. An algorithm for 3D simulation of branchwork karst networks using Horton parameters and A* Application to a synthetic case. In J. Garland, J. E. Neilson, S. E. Laubach, and K. J. Whidden, editors, *Advances in Carbonate Exploration and Reservoir Analysis*, volume Special Publications, 370, pages 295–306. Geological Society, London, 2012.

Fabien Cornaton and Pierre Perrochet. Analytical 1D dual-porosity equivalent solutions to 3D discrete single-continuum models. application to karstic spring hydrograph modelling. *Journal of Hydrology*, 262(1):165–176, 2002.

W. Dreybrodt, F. Gabrovsek, and D. Romanov. *Processes of speleogenesis: a modeling approach*. Carsologica. Editions Zalozba, 2002.

Derek Ford and Paul D Williams. *Karst hydrogeology and geomorphology*. John Wiley & Sons, 2013.

Daniel Fraiman, Pablo Balenzuela, Jennifer Foss, and Dante R Chialvo. Ising-like dynamics in large-scale functional brain networks. *Physical Review E*, 79(6):061922, 2009.

Christopher G. Groves and Alan D. Howard. Early development of karst systems 1. Preferential flow path enlargement under laminar flow. *Water Resources Research*, 30(10):2837–2846, 1994.

A Hartmann, N Goldscheider, T Wagener, J Lange, and M Weiler. Karst water resources in a changing world: Review of hydrological modeling approaches. *Reviews of Geophysics*, 52(3):218–242, 2014.

Christophe P Haynes and Anthony P Roberts. Generalization of the fractal Einstein law relating conduction and diffusion on networks. *Physical Review Letters*, 103(2):020601, 2009.

Martin Hendrick and Philippe Renard. Fractal dimension, walk dimension and conductivity exponent of karst networks around Tulum. *Frontiers in Physics*, 4:27, 2016.

Melissa E Hill, Mark T Stewart, and Angel Martin. Evaluation of the modflow-2005 conduit flow process. *Ground Water*, 48 (4):549–559, 2010.

Haye Hinrichsen. Non-equilibrium critical phenomena and phase transitions into absorbing states. *Advances in physics*, 49(7): 815–958, 2000.

Alan D Howard and Christopher G Groves. Early development of karst systems, 2, turbulent flow. *Water Resources Research*, 31(1):19–26, 1995.

O. Jaquet, P. Siegel, G. Klubertanz, and H. Benabderrhamane. Stochastic discrete model of karstic networks. *Advances in Water Resources*, 27(7):751–760, 2004.

PY Jeannin, C Groves, and P Häuselmann. Speleological investigations. *Oldscheider N. & Drew D.(eds.), Methods in Karst Hydrogeology, Taylor & Francis*, pages 25–44, 2007.

Hervé Jourde, Fabien Cornaton, Séverin Pistre, and Pascal Bidaux. Flow behavior in a dual fracture network. *Journal of Hydrology*, 266(1):99–119, 2002.

Ana M Juarez. Ecological degradation, global tourism, and inequality: Maya interpretations of the changing environment

in quintana roo, mexico. *Human Organization*, 61(2):113–124, 2002.

Leo P Kadanoff. Theories of matter: infinities and renormalization. *arXiv preprint arXiv:1002.2985*, 2010.

Gregory Kaeser. *Groundwater Flow and Solute Transport Modeling in the Karst System Ox Bel Ha, Tulum (Mex).* MSc. thesis. Hydrogeologie et Geothermie. Universit de Neuchtel, 2016.

Patricia N Kambesis and James G Coke IV. Overview of the controls on eogenetic cave and karst development in Quintana Roo, Mexico. In *Coastal Karst Landforms*, pages 347–373. Springer, 2013.

Mehran Kardar. *Statistical physics of fields.* Cambridge University Press, 2007.

Mehran Kardar and Yi-Cheng Zhang. Scaling of directed polymers in random media. *Physical Review Letters*, 58(20):2087, 1987.

Mehran Kardar, Giorgio Parisi, and Yi-Cheng Zhang. Dynamic scaling of growing interfaces. *Physical Review Letters*, 56(9): 889, 1986.

NC Kenkel and DJ Walker. Fractals in the biological sciences. *Coenoses*, 11(2):77–100, 1996.

L Kiraly. Rapport sur l'état actuel des connaissances dans le domaine des caractères physiques des roches karstiques. *Hydrogeology of karstic terrains*, (3):53–67, 1975.

Sari B Kusumayudha, MT Zen, Sudarto Notosiswoyo, and Rudy Sayoga Gautama. Fractal analysis of the oyo river, cave systems, and topography of the gunungsewu karst area, central Java, Indonesia. *Hydrogeology Journal*, 8(3):271–278, 2000.

Michael J Lace and John E Mylroie. *Coastal karst landforms*. Springer Science & Business Media, 2013.

Lev Davidovich Landau and Evgenii Mikhailovich Lifshitz. *Course of theoretical physics*. Elsevier, 2013.

Martin Laverty. Fractals in karst. *Earth Surface Processes and Landforms*, 12(5):475–480, 1987.

Rudolf Liedl, Martin Sauter, Dirk Hückinghaus, Torsten Clemens, and Georg Teutsch. Simulation of the development of karst aquifers using a coupled continuum pipe flow model. *Water Resources Research*, 39(3), 2003.

Benoit B Mandelbrot. *The fractal geometry of nature*, volume 173. Macmillan, 1983.

Robert Manning, John Purser Griffith, TF Pigot, and Leveson Francis Vernon-Harcourt. *On the flow of water in open channels and pipes*. 1890.

Nicos Martys, Marek Cieplak, and Mark O Robbins. Critical phenomena in fluid invasion of porous media. *Physical Review Letters*, 66(8):1058, 1991.

Zeev Olami, Hans Jacob S Feder, and Kim Christensen. Self-organized criticality in a continuous, nonconservative cellular automaton modeling earthquakes. *Physical Review Letters*, 68(8):1244, 1992.

Arthur N Palmer. Origin and morphology of limestone caves. *Geological Society of America Bulletin*, 103(1):1–21, 1991.

E. Pardo-Iguzquiza, P. A. Dowd, C. S. Xu, and J. J. Duran-Valsero. Stochastic simulation of karst conduit networks. *Advances in Water Resources*, 35:141–150, 2012.

Eulogio Pardo-Iguzquiza, Juan J Durán-Valsero, and Victor Rodríguez-Galiano. Morphometric analysis of three-dimensional networks of karst conduits. *Geomorphology*, 132 (1):17–28, 2011.

Romualdo Pastor-Satorras and Daniel H Rothman. Scaling of a slope: the erosion of tilted landscapes. *Journal of Statistical Physics*, 93(3-4):477–500, 1998.

Sona Prakash, Shlomo Havlin, Moshe Schwartz, and H Eugene Stanley. Structural and dynamical properties of long-range correlated percolation. *Physical Review A*, 46(4):R1724, 1992.

Gunnar Pruessner. *Self-organised criticality: theory, models and characterisation*. Cambridge University Press, 2012.

Sidney Redner. Fractal and multifractal scaling of electrical conduction in random resistor networks. In *Mathematics of Complexity and Dynamical Systems*, pages 446–462. Springer, 2012.

Ph Renard and G De Marsily. Calculating equivalent permeability: a review. *Advances in water resources*, 20(5):253–278, 1997.

Andrea Rinaldo, Jayanth R Banavar, and Amos Maritan. Trees, networks, and hydrology. *Water Resources Research*, 42(6), 2006.

Ignacio Rodríguez-Iturbe and Andrea Rinaldo. *Fractal river basins: chance and self-organization*. Cambridge University Press, 2001.

Michael J. Ronayne. Influence of conduit network geometry on solute transport in karst aquifers with a permeable matrix. *Advances in Water Resources*, 56:27–34, June 2013. doi: 10.1016/j.advwatres.2013.03.002.

Michael J. Ronayne and Steven M. Gorelick. Effective permeability of porous media containing branching channel networks. *Phys Rev E Stat Nonlin Soft Matter Phys*, 73(2 Pt 2):026305, 2006.

Muhammad Sahimi. *Flow and transport in porous media and fractured rock: from classical methods to modern approaches*. John Wiley & Sons, 2011.

A Schiller, I Schattauer, R Supper, K Motschka, and GA Merediz. Advanced processing of airborne fdem data for improved imaging of karst conduit networks in the region of Tulum, Mexico. In *First European Airborne Electromagnetics Conference*, 2015.

Jörg Siemers and Wolfgang Dreybrodt. Early development of karst aquifers on percolation networks of fractures in limestone. *Water Resources Research*, 34(3):409–419, 1998.

RF Smalley, Donald Lawson Turcotte, and Sara A Solla. A renormalization group approach to the stick-slip behavior of faults. *Journal of Geophysical Research: Solid Earth*, 90(B2): 1894–1900, 1985.

Peter L Smart, Patricia A Beddows, Jim Coke, Stefan Doerr, Samantha Smith, and Fiona F Whitaker. Cave development on the caribbean coast of the yucatan peninsula, quintana roo, mexico. *Geological Society of America Special Papers*, 404:105–128, 2006.

Chaoming Song, Shlomo Havlin, and Hernan A Makse. Self-similarity of complex networks. *Nature*, 433(7024):392–395, 2005.

Chaoming Song, Lazaros K Gallos, Shlomo Havlin, and Hernán A Makse. How to calculate the fractal dimension of a complex network: the box covering algorithm. *Journal of Statistical Mechanics: Theory and Experiment*, 2007(03): P03006, 2007.

Didier Sornette. *Critical phenomena in natural sciences: chaos, fractals, selforganization and disorder: concepts and tools*. Springer Science & Business Media, 2006.

H Eugene Stanley and Antonio Coniglio. Flow in porous media: The" backbone" fractal at the percolation threshold. *Physical Review B*, 29(1):522, 1984.

Colin P. Stark. An invasion percolation model of drainage network evolution. *Nature*, 352(6334):423–425, 1991. doi: 10.1038/352423a0.

Dietrich Stauffer and Ammon Aharony. *Introduction to percolation theory*. CRC press, 1994.

Olaf Stenull and Hans-Karl Janssen. Noisy random resistor networks: Renormalized field theory for the multifractal moments of the current distribution. *Physical Review E*, 63(3): 036103, 2001.

Gilbert Strang. A framework for equilibrium equations. *SIAM Review*, 30(2):283–297, 1988.

Uwe C Täuber. *Critical dynamics: a field theory approach to equilibrium and non-equilibrium scaling behavior*. Cambridge University Press, 2014.

Tamás Vicsek. *Fractal growth phenomena*, volume 2. World Scientific, 1992.

Kenneth G. Wilson. Renormalization group and critical phenomena. ii. phase-space cell analysis of critical behavior. *Phys. Rev. B*, 4:3184–3205, Nov 1971. doi: 10.1103/PhysRevB.4.3184. URL `http://link.aps.org/doi/10.1103/PhysRevB.4.3184`.

Jean Zinn-Justin. *Phase transitions and renormalization group*. Oxford University Press on Demand, 2007.